

# 國立交通大學

## 物理研究所

### 碩士論文

矽晶表面上氫和氯原子的換位運動觀察與熱力學研究

Kinetics of Position Exchange between H and Cl Atomic

Sites on a Chlorine terminated Si Surface



研 究 生：鄭閔光

指導教授：林登松 教授

中華民國九十六年六月

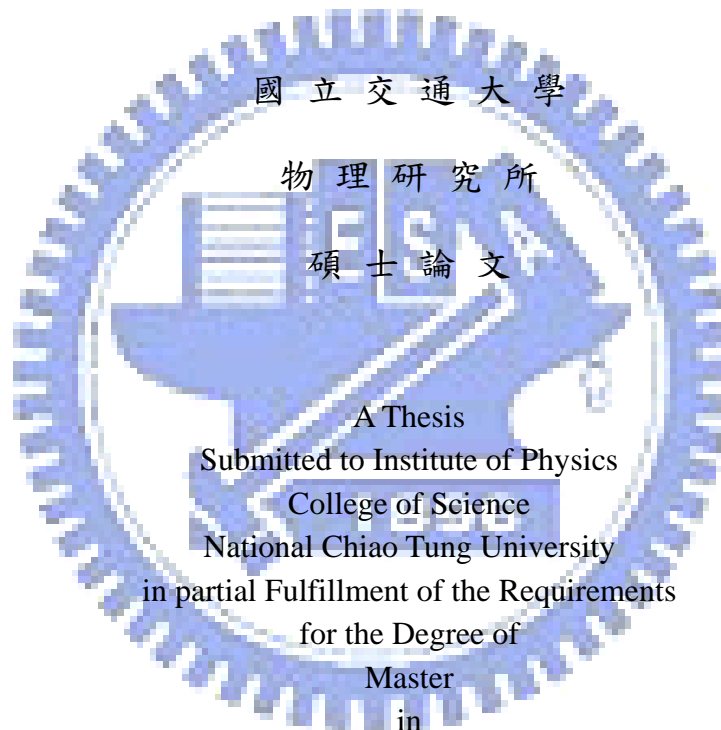
矽晶表面上氫和氯原子的換位運動觀察與熱力學研究  
Kinetics of Position Exchange between H and Cl Atomic  
Sites on a Chlorine terminated Si Surface

研 究 生：鄭閔光

Student：Min-Kuang Cheng

指導教授：林登松

Advisor：Deng-Sung Lin



Physics

June 2007

Hsinchu, Taiwan, Republic of China

中華民國九十六年六月

# 矽晶表面上氫和氯原子的換位運動觀察與熱力學研究

學生：鄭閃光

指導教授：林登松 教授

國立交通大學物理研究所碩士班

## 摘 要

利用掃描穿隧顯微鏡(STM)，本論文報導我們在 Si(100)-(2×1):Cl 樣品表面上氯和氯原子的換位運動觀察與其熱力學的探討。首先，我們觀察原本存在 Si(100)-(2×1):Cl 表面上的“Cl 位置”缺陷”並進一步觀察這種”缺陷”於樣品溫度 570~650K 之間的移動現象，我們發現這種缺陷有兩種動態，一種是沿著 dimer row 方向產生跳動稱為 inter-dimer 跳躍、另一種則是在同一個 dimer 內跳動稱為 intra-dimer 跳躍。接著我們曝上氫原子於 Si(100)-(2×1):Cl 表面。在 570 K 時，氫原子幾乎很少移動或久久移動一次，但當溫度增加到 650K 時，氫原子移動的速度較溫度在 570K 時快，並且在兩張影像間已有多次跳躍的現象發生。這些現象和移動的速度跟未曝氫原子於表面時所比較是相吻合的。由 Arrhenius 關係線，我們推算出氫-氯原子交換運動的動力能障，即對於曝氫而言 inter-dimer 跳躍的動力能障為 1.23 eV、至於 intra-dimer 跳躍的動力能則為 0.70 eV，相對的，在對於沒有曝氫的 inter-dimer 跳躍的動力能為 1.14 eV，intra-dimer 跳躍的動力能則是 0.62eV。從此結果我們可以更加的確定在未曝氫的 Si(100)-(2×1):Cl 表面上產生移動的”缺陷”是樣品處理中殘留的氫原子或  $Cl_2$  氣體中殘存的 HCl 分子吸附。

# Kinetics of Position Exchange between H and Cl Atomic Sites on a Chlorine terminated Si Surface

**Student: Min-Kuang Cheng**

**Adviser: Dr. Deng-Sung Lin**

**Institute of Physics  
National Chiao Tung University**

## Abstract

We have observed in real-time the motion and behavior of hydrogen atoms on Cl-saturated Si(100)-(2x1) surfaces with temperatures ranging from 570 to 650 K using ultra-high vacuum variable-temperature scanning tunneling microscopy (STM). We have taken STM movies with and without additional exposure of hydrogen atoms onto the Cl-terminated surface. The STM images show that there were two types of H-Cl exchange movement: inter-dimer and intra-dimer. By observing the H-exposed Cl sample we traced the movements of H sites. At 570K, hydrogen atoms seldom moved and their motions were mainly single jumps. As the temperature increases, the frequency of the movement becomes higher. At 650K, hydrogen atoms move at a fast pace and multiple jumps dominate in our sequential images. We obtained similar results from the non H-exposed Cl sample. By plotting the Arrhenius relations we were able to obtain the activation energies for each set. From the set with H-exposure we obtained  $1.23\text{eV}$  for inter-dimer hoppings and  $0.70\text{eV}$  for intra-dimer hoppings respectively, while for the set without H-exposure we obtained  $1.14\text{eV}$  and  $0.62\text{eV}$  for the inter-dimer and intra-dimer hoppings respectively. Therefore, we were able to confirm from these results that the vacancies we have seen moving on the non H-exposed Si(100) Cl-terminated surface as the residual hydrogen atoms got on the surface during sample preparation and/or from the  $\text{HCl}$  impurities in the  $\text{Cl}_2$  gas source.

## Acknowledgment

經過了這麼多事，如今終於順利的畫上句點，雖然有些感慨，更有許多不捨，其中有許多感受是無法用言語來表達的，但我還是想對許多人致上我由衷的感謝。

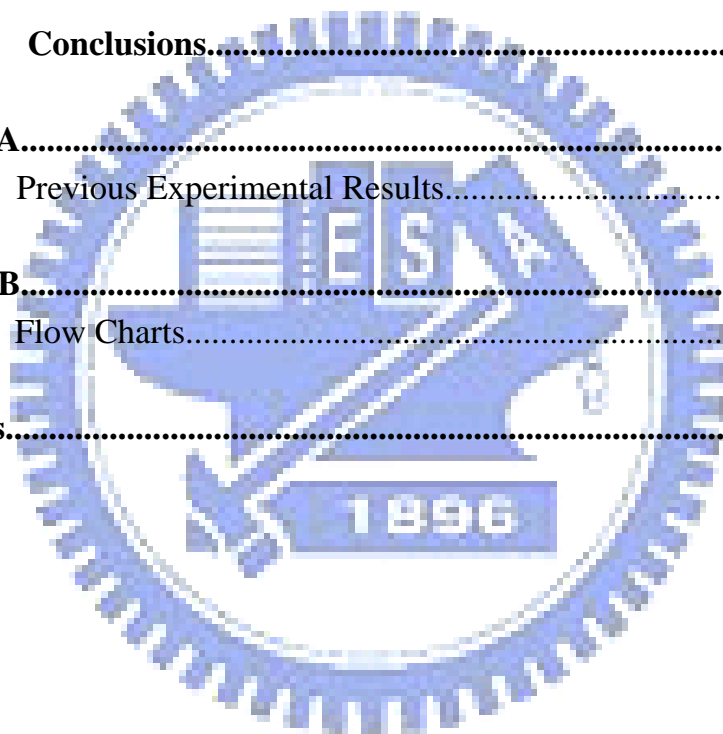
首先，我要感謝的自然是影響我最深的人，我的指導教授林登松老師，感謝他給我這個機會成為他的學生，在他的身邊學習的這段時間，我學到如何用更嚴謹仔細的態度做事，相信這些收穫足以讓我受用一生，於此再度向老師獻上最深的謝意！此外，我也要感謝口試委員蔡秀芬老師和張正宏老師給予我論文上的指正及寶貴意見；而此論文得以順利完成，實驗室裡的夥伴們更是功不可沒，尤其要特別感謝明峰學長，倘若沒有他的幫忙，此論文恐怕難以完成；同時，也感謝鎧銘學長、世鑫學長以及依亭的協助，幫我解決了許多實驗上的困難，並解開了我理論上的疑問，很高興能和你們同在一個實驗室裡，否則我可能會一直陷在問題無法解決的輪迴裡。再來，要感謝曉婷總是讓實驗室保持著愉快的氣氛，舒緩了不少的壓力；同時，更要感謝乾庭、仁陽和瑞仁在求學過程中對我的支持與鼓勵，也讓我對臺灣有了更深的瞭解；還有謝謝德明、奎霖和其他的同學們，認識你們是一種緣份，也謝謝學弟中廷與展源的幫助與鼓勵，感謝所有曾經幫助過我的人。

最後，要感謝我的家人，謝謝父母用心良苦的栽培和生活上的支持，以及奶奶平日對我的細心照顧，弟弟坤毅的鼓勵，與女友夢竹的陪伴和勉勵，陪我一起渡過這段珍貴又重要的日子，謝謝大家！

# Contents

摘要.....	i
Abstract.....	ii
Acknowledgements.....	iii
Contents.....	iv
<b>Chapter 1 Introduction.....</b>	<b>1</b>
<b>1.1 Motivation.....</b>	<b>1</b>
<b>1.2 The Clean Si(100)-(2x1) Surface.....</b>	<b>3</b>
<b>1.3 Vacancy Structure.....</b>	<b>8</b>
<b>1.4 Diffusion Mechanisms.....</b>	<b>13</b>
1.4.1 Data Analysis.....	14
1.4.1.1 Unrestricted Random Walk.....	14
1.4.1.2 Arrhenius Relations.....	16
1.4.1.3 Jump Length Distributions.....	18
1.4.2 Transport Mechanisms.....	19
1.4.2.1 Hopping Mechanism.....	19
1.4.2.2 Vacancy-Mediated Diffusion Mechanism.....	20
1.4.2.3 Exchange Mechanism.....	21
<b>1.5 Literature Reviews.....</b>	<b>22</b>
1.5.1 Cl-terminated Si(100)-(2x1) Surface.....	22
1.5.2 Case Studies-Vacancy Diffusions.....	24
1.5.3 Enhancement of surface diffusion with adsorbed H.....	29
1.5.4 Cl Extraction by H-atoms from Cl-terminated Si(100) Surface.....	30
<b>Chapter 2 Experimental Setup.....</b>	<b>34</b>
<b>2.1 The Vacuum System.....</b>	<b>34</b>
<b>2.2 Scanning Tunneling Microscope (STM).....</b>	<b>36</b>
2.2.1 An Introduction.....	36
2.2.2 The STM System.....	37
2.2.3 Principles of Electron Tunneling.....	38
<b>2.3 Tip Preparation.....</b>	<b>40</b>
<b>2.4 Sample Preparation.....</b>	<b>42</b>

<b>Chapter 3 Results and Discussion.....</b>	<b>43</b>
<b>3.1 The Dynamics of H-Hopping.....</b>	<b>45</b>
3.1.1 Motion of H atoms at Various Temperatures.....	45
3.1.2 Arrhenius Plot and Activation Energy for the H-exposed Set.....	59
<b>3.2 Statistics of H-exposed Hoppings.....</b>	<b>61</b>
3.2.1 Raw Data.....	61
3.2.2 Preference of Hopping Movements.....	63
<b>3.3 Results on Non H-exposed Hoppings.....</b>	<b>70</b>
<b>3.4 Conclusion.....</b>	<b>73</b>
 <b>Chapter 4 Conclusions.....</b>	 <b>74</b>
 <b>Appendix A.....</b>	 <b>76</b>
A.1 Previous Experimental Results.....	76
 <b>Appendix B.....</b>	 <b>79</b>
B.1 Flow Charts.....	79
 <b>References.....</b>	 <b>83</b>



# Chapter 1 Introduction

## 1.1 Motivation

Surface defect often plays an important role in thin-film growth processes. Defects, such as, vacancies, steps, and anti-phase domain boundaries, is the key factors in the evolution of surface morphology in the past few decades. In order to control particular surface morphologies, we need to achieve a thorough understanding of the balance between the thermodynamics and various atomic-scale kinetic processes. The equilibrium of surface morphologies can be achieved by the control of the binding or configurational free energies, which is the thermodynamics, while the rates at which the dynamic events occur on the surface are governed by the surface energy barriers or the activation barrier, that is, the kinetics.

For long, there has been much interest about the early stages of the epitaxial growth on Si(100)-(2x1) surface. It wasn't only because of its technological importance, but also due to its relatively simple structure. The properties of the Si(100) surface have been under extensive studies recently, more about its equilibrium structures and surface kinetic processes has been investigated. The interaction of the Si adatoms on the surface leads to interesting issues. It is known that the top-layer atoms of the Si(100) surface dimerize (as two surface atoms binding together to form a dimer) to reduce the number of dangling bonds. This establishes two characteristic directions on the surface, along the dimer row and perpendicular to the dimer. The parallel rows of the dimer bonds also reduce the overall surface energy. Surface vacancy contains two kinds, a single-atom (monomer) vacancy, and a two-joint atom (dimer) vacancy. The abundance of surface dimer vacancies and vacancy clusters on the Si(100)-(2x1) surface has been recognized since the surface was first observed with a scanning tunneling microscope (STM) [1]. Theoretical studies have concluded that vacancy formation is mediated by surface strain relaxation and the reduction of the dangling bonds [2-3]. There are also experimental studies on the structure and kinetics of the vacancies on this surface still happening to date. The kinetics and the thermal behavior of the surface vacancy play a big part in both growth and etching, and several recent experiments using scanning tunneling microscope have now provided some insights into the atomic level structural evolution related to the growth on Si(100) surfaces. As we gain more insights into the phenomenon of chemical growth and etching, there are still some questions regarding the surface vacancies need to be considered. The vacancies used to be thought of as atoms missing from the surface and vacancy diffusions are just atoms migrating from the binding sites to the nearest empty (vacant) bind sites on a static



substrate through a series of uncorrelated displacements over the minimum energy barrier so it seems as the vacancy is moving. But now we have every reason to believe that the “vacancies” are just the residual gas atoms, and this lead us to believe that surface diffusions of the “vacancies” is actually the exchange between the deposited atoms and the residual gas atoms already on the surface. In order to prove our suspicion, we deposited chlorine(Cl) on Si(100)-(2x1) surface and focus on the Cl-terminated silicon surface in real time via atomic scale imaging by using scanning tunneling microscopy. The purpose of our study is to gain a better understanding and further insight in the microscopic dynamical behavior of surface diffusions.



## 1.2 The Clean Si(100)-(2x1) Surface

Silicon crystal has been used by many other researches for decades, and its properties are fairly well examined. Due to its relatively simple structure, and its importance, Si(100) is being used in our experiment. In this section, we will be discussing about the details of the Si(100)-(2x1) surface structure.

As a group IV element, silicon has four electrons in its outer orbit. In a silicon crystal, each silicon atom has four valance bonds bonded to four neighboring silicon atoms in tetrahedral form. The crystal structure of silicon is a diamond structure with a lattice constant of 5.43 Å, as shown in Fig. 1.1.

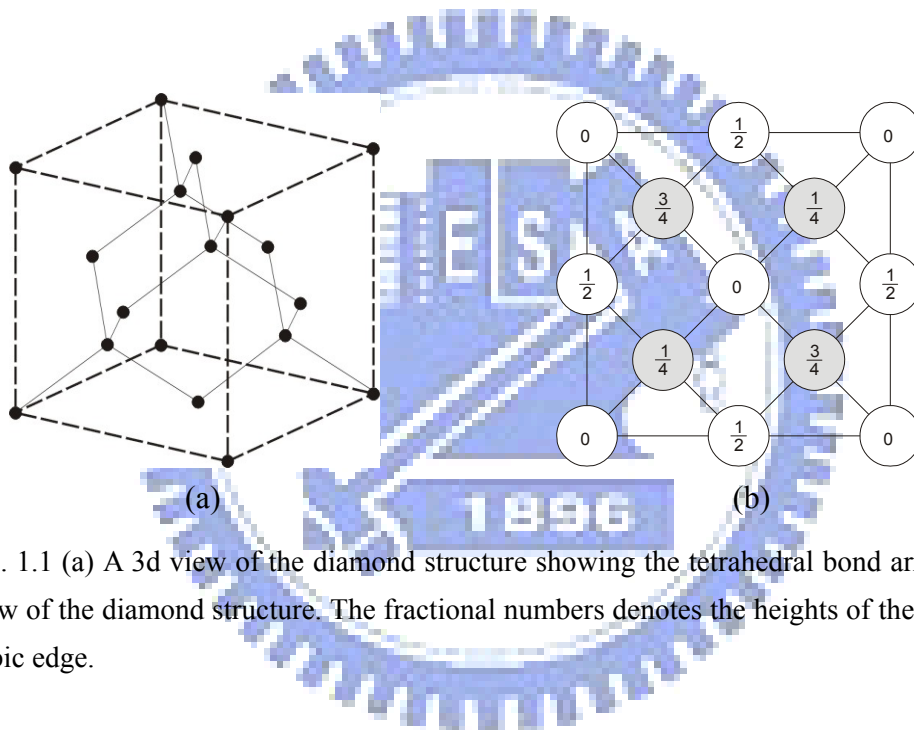


Fig. 1.1 (a) A 3d view of the diamond structure showing the tetrahedral bond arrangement. (b) Top view of the diamond structure. The fractional numbers denotes the heights of the atoms in units of a cubic edge.

When the silicon crystal is cleaved along a different crystal orientation, the new surface will reconstruct itself into a different surface atomic structure. For example, if the crystal is cleaved along the (100) direction, the exposure surfaces will reconstruct into a (2x1) structure. If the crystal is cleaved along the direction normal to the (111) direction, the new surface will then be reconstruct into a (7x7) structure. This is one of the properties of silicon. For the convenience, Si(100)-(2x1) surface is a good choice to operate on.

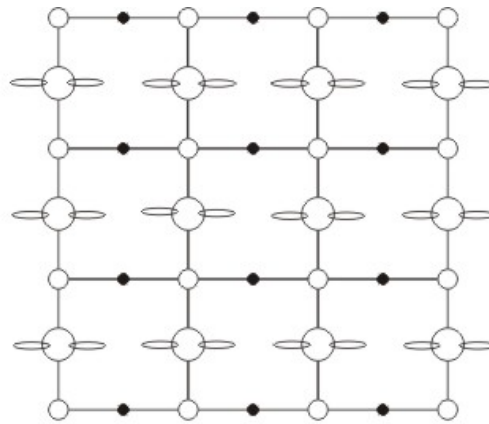
If one cleaves through the silicon crystal along the (100) direction, two valence bonds of each Si atom at the exposed surface will break up and transform into dangling bonds. Therefore, every silicon atoms in the surface will have two dangling bonds and two valence bonds, as shown in Fig. 1.2.



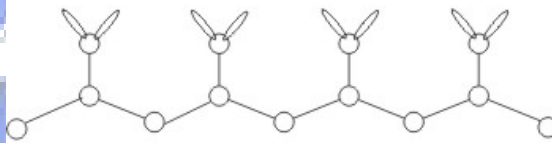
Fig. 1.2 The side view of an ideal Si(100) surface. Each silicon atom has two valence bonds and two dangling bonds.

Figure 1.3 displays the top view of this unreconstructed Si(100) surface with (1x1) structure. In this (1x1) structure, the density of the dangling bonds is high (two dangling bonds per atom), and therefore making the surface energy high and causing the (1x1) structure to be unstable. To make the structure more stable, one needs to reduce the number of dangling bonds. In doing so, the first layer atoms in the surface will need to be reconstructed. Only in this way can the surface energy be lowered and the (1x1) structure more stable.

Upon reconstruction, two neighboring atoms form a strong sigma ( $\sigma$ ) bond by joining one of the two drifting dangling bonds. The total amount of dangling bonds on the cleaved surface is then reduced by fifty percent. The remaining dangling bonds can then be further forming a weak pi ( $\pi$ ) bond, as shown in Fig. 1.4. The (1x1) structure of the surface is now transformed into a (2x1) structure, as shown in Fig. 1.5. The newly formed bonding pairs of silicon atoms are called ‘dimers’.



(a) top view



(b) side view

Fig. 1.3 (a) The top view of an ideal Si(100)-(1x1) surface structure.  $\circ$  : the first layer atoms;  $\bullet$  : the second layer atoms;  $\bullet$  : the third layer atoms. (b) The side view of the surface structure.

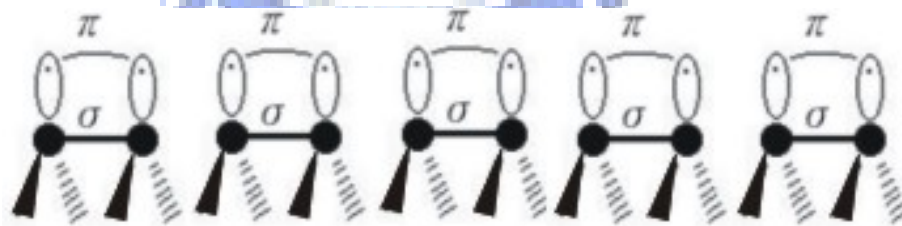
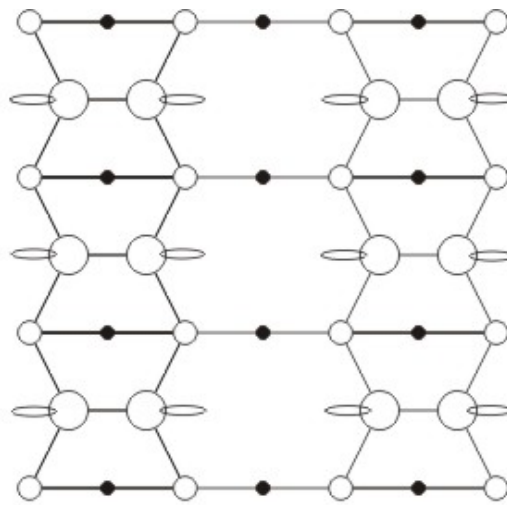
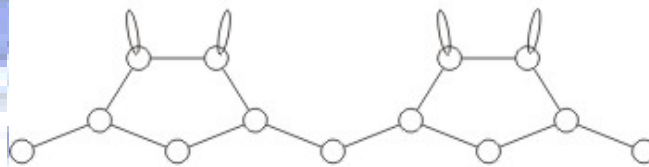


Fig. 1.4 The side view of the first layer of the constructed Si(100)-(2x1) surface structure showing the pi ( $\pi$ ) bond and the sigma ( $\sigma$ ) bond.



(a) top view



(b) side view

Fig. 1.5 The top view (a) and the side view (b) of an Si(100)-(2x1) reconstructed surface structure.  $\bigcirc$  : the first layer atoms.  $\circ$  : the second layer atoms.  $\bullet$  : the third layer atoms.

When we cleave through the silicon surface along the (100) direction, a step structure is formed, as shown in Fig. 1.6. The height of the step is about  $1.36\text{\AA}$ . Since the dimer rows on the neighboring terraces are perpendicularly oriented, thus the steps are divided into two different types. Type one, called  $S_A$ , are the steps where the dimer row direction on the upper terrace parallels to the step edge. Type two, called  $S_B$ , are the steps where the dimer row direction on the upper terrace is perpendicular to the step edge.

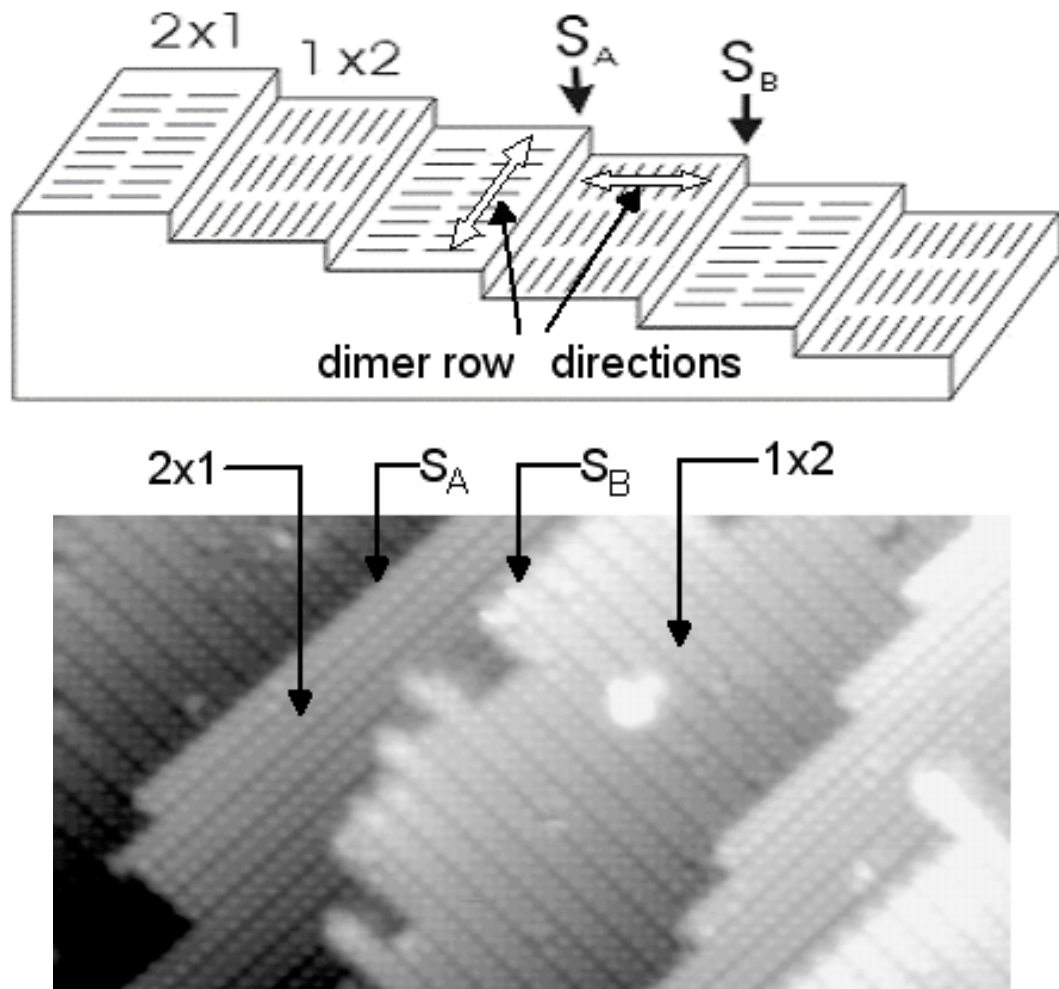


Fig. 1.6 The step structure of  $S_A$  and  $S_B$  on the Si(100)-(2x1) surface. The top picture shows the different directions of the dimer rows in both  $S_A$  and  $S_B$  steps.  $S_A$  is the step where the dimer row direction of the upper terrace parallels to the step edge.  $S_B$  is the step where the dimer row direction of the upper terrace is perpendicular to the step edge. The bottom picture is a STM image of the steps. The size of the image taken is  $200 \times 100 \text{ \AA}^2$ , with a sample bias of +2V.

### 1.3 Vacancy Structure

In all elements, atoms align together to form a distinct pattern in a crystal surface. Vacancies are defects in the crystal surface. This happens when there are atoms missing from the perfectly aligned crystal patterns, as shown in Fig.1.7. The missing atoms could have been moved from their original sites into other neighboring sites, in which they fill the pre-empty sites, or simply replace themselves with the preoccupying atoms. The proceedings mentioned above are what we call surface diffusion, which we will get into details later. So the empty sites left are called vacancies, and it is a very common event in all epitaxial growth or chemical etching fabrication processes.

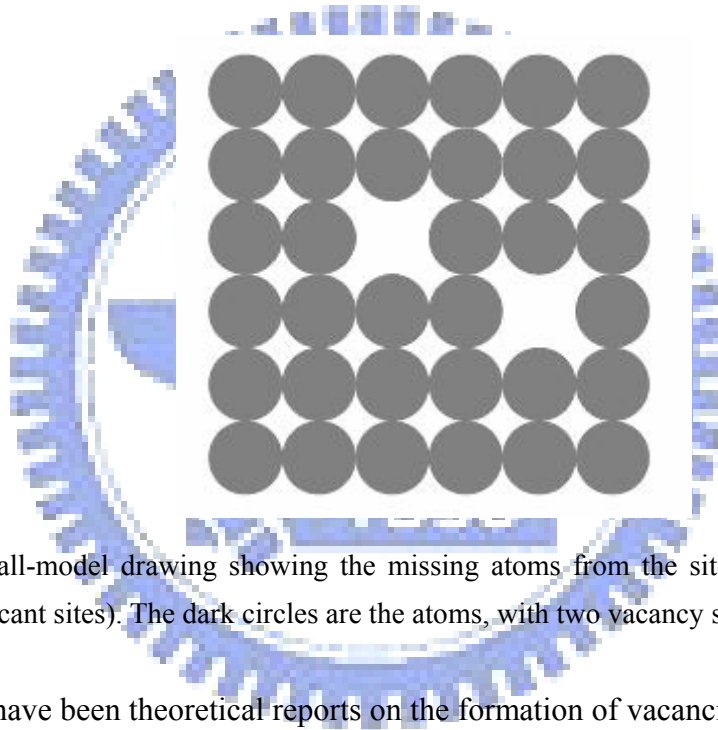


Fig. 1.7 A ball-model drawing showing the missing atoms from the sites, leaving behind empty spaces (or vacant sites). The dark circles are the atoms, with two vacancy sites present.

There have been theoretical reports on the formation of vacancies in the past few years, and in the reports they concluded that surface strain relaxation and the reduction of the dangling bonds improve the formation of vacancies [2-3]. Vacancies are very important to surface morphologies. It plays a key role in thin-film growth processes and chemical etching processes. It is known that on semiconductor surfaces, in order to make a growing crystal on the surface to be smooth, it is often operated under high activation temperatures, typically a ratio between the activation and melting temperature well above the order of 0.5 ( $T_{act}/T_{melt} > 0.5$ ). Growing at lower temperatures typically results in a rough surface morphology. This has attracted number of interests and there have been reports discussing about the improvements under low activation temperatures and the diffusion mechanisms with low activation energies. So, in order to control particular surface morphologies, it is important to achieve an understanding of the balance between the thermodynamics and the

various atomic-scale kinetic processes, which is the dynamic events happening on the surface, and with one of them, namely, is the vacancy diffusions.

There are two kinds of vacancies, a single vacancy, where a single atom is missing from the site, and a dimer vacancy, where a pair of two-joint atoms is missing in a dimer site along the dimer row. Single vacancies (SV) are the smallest defect one can find on the crystal surface. Although it might not be found on a clean silicon surface, but once the surface is been reconstructed, number of single vacancies starts to appear, and it is then very easily find. As mentioned, atoms join to form bonds in order to reduce the total surface energies. And in the process, there will be atoms tending to escape from the first layer of the surface structure, leaving behind an empty site. If these sites were not filled, it becomes a vacancy site. That is why on reconstructed silicon (2x1) surface it has so many single vacancy sites present. Following is a STM image showing the Si(100)-(2x1) Cl-terminated surface. From the image it shows the vacancy sites in the perfectly aligned dimer rows. The white arrow indicates a single vacancy site where the silicon atom is missing from the site. The corresponding surface structure with a missing Si atom in the Si(100)-(2x1) Cl-terminated surface is shown on the right.

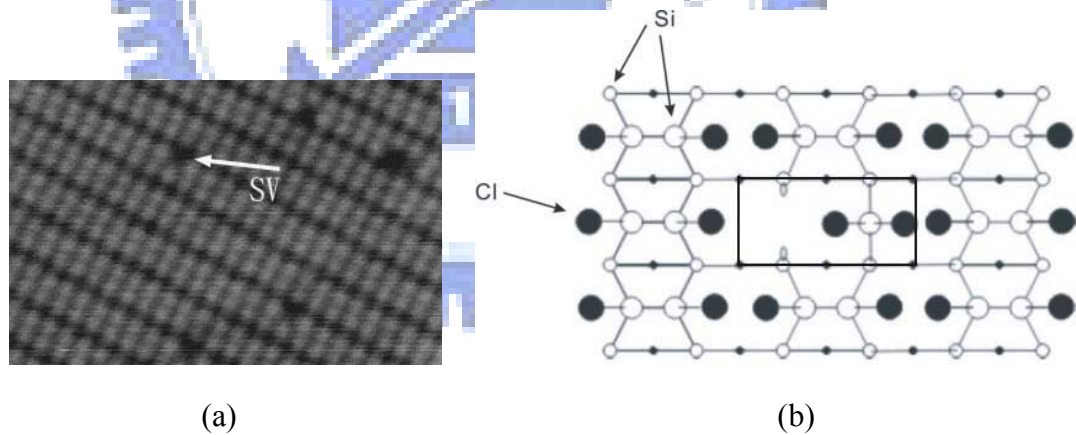


Fig. 1.8 (a) STM image of the Si(100)-(2x1) Cl-terminated surface. A single vacancy is marked by the white arrow. (b) The corresponding dimer structure of a SV on the Si(100)-(2x1) Cl-terminated surface. It shows a missing Si atom from the structure thus forming a single vacancy. The dimer is framed. The STM image was taken with positive sample bias.



For the dimer defect, where the two adjacent atoms have gone missing, leaving behind an empty dimer space among the dimer row occasionally happens in the crystal surface. The two monomers join together to form a dimer in the surface, and sometimes both atoms move together, jumping from one dimer site to another along the dimer row. This type of vacancy is called dimer vacancy, and the jumping mechanism is called dimer diffusion. There are three primitive types of dimer vacancy defects. These are the single missing-dimer vacancy structure (1-DV), two adjacent missing-dimer vacancy clusters (2-DV), and three adjacent missing-dimer vacancy clusters (3-DV) respectively. Theoretical study shows that the reconstructed structure of dimer vacancies is in the ground state, whereas the unreconstructed structure is in the meta-state with weaker pi bonds, and the formation energy is higher by 0.4eV [3].

From the experiment done by J.Wang and co., with a perfectly dimerized Si(100) surface, under the meta-stable configuration, the formation energy for a DV structure is 0.64eV/dimer. In the stable configuration, which involves rebonding, has a formation energy of 0.22eV/dimer. The 2-DV cluster, formed by removing two adjacent dimers from the Si(100) surface, has a formation energy of 0.33eV, or 0.16 eV/dimer under stable configuration. That is lower than the formation energy for the stable structure of a 1-DV with 0.22eV/dimer. For the 3-DV cluster, formed by removing three adjacent dimers from the Si(100) surface, has a formation energy of 0.45eV (0.15eV/dimer) in the stable configuration. Again, lower than the formation energy for the stable structure of a 1-DV. Figure 1.9 shows the unreconstructed and the reconstructed structures of 1-DV on a clean Si(100)-(2x1) surface. Figure 1.10 shows a 2-DV defect, containing two dimer vacancies in the neighboring sites in the same row. The formation of a 2-DV from two isolated DVs requires an energy of 0.11eV.

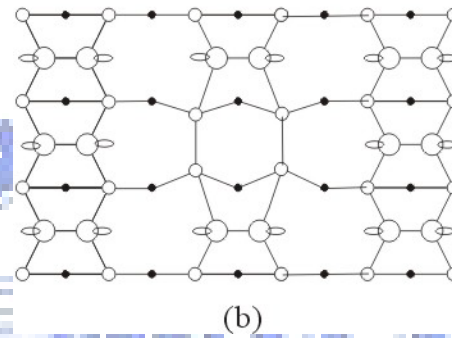
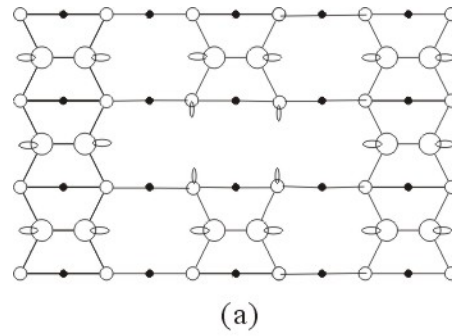


Fig. 1.9 Schematic representation of an atomic configurations of a DV on the clean Si(100)-(2x1) surface. (a) is the unreconstructed DV structure, and is meta-stable. (b) is the reconstructed DV structure, which is stable.

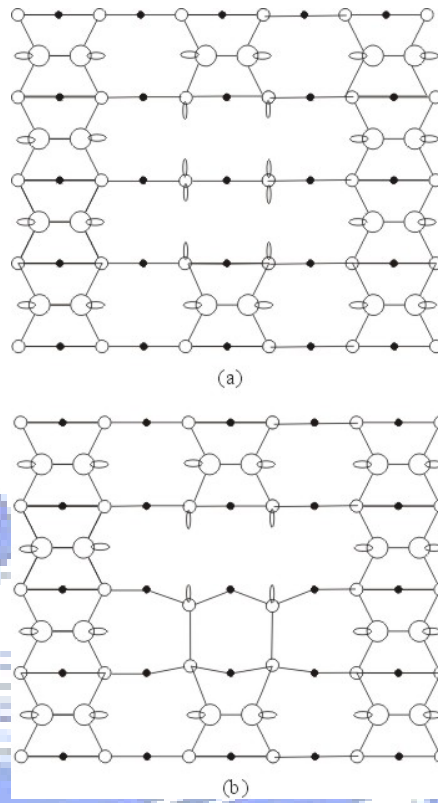


Fig. 1.10 Schematic representation of an atomic configurations of a 2-DV on the clean Si(100)-(2x1) surface. (a) is the unreconstructed 2-DV structure, and is meta-stable. (b) is the reconstructed 2-DV structure, which is stable.

## 1.4 Diffusion Mechanisms

Interactions between individual atoms has always being interesting in the history of surface science. The migration of individual atoms across the solid surfaces and their aggregation into cluster nuclei are among the most fundamental interactions in the field. It is becoming more and more important as scientists and engineers attempting to develop new materials by controlling their growth at the atomic level. Most of the manufactured products are made from atoms. The property of these products depends on how those atoms are arranged. For example, the arrangement of atoms in diamond is different to the arrangement of atoms in coal, but, if we rearrange the atoms in coal then we can make diamond. If we can rearrange the atoms in sand, and with the addition of few other raw elements, we will have a computer chip in our hand, and so on. In the sense of the recent arise of the so called nanotechnologies, an improvement of material properties to make it stronger, lighter and more concise in the evolution of the new generation of products. It is therefore important to get a detailed understanding of the basic atomic-level crystal and epitaxial growth processes. In order to develop a realistic model for the material fabrication process, it is necessary to determine quantitatively the relative energetics of the individual atoms as they migrate across the perfectly formed crystal planes, being cooperated into the top layer of surface atoms, interact with various surface defects, or combine to form cluster nuclei.

The technique of scanning tunneling microscopy has allowed us to view individual atoms and track their motions as they move across a well-defined crystal surface. From the details of the atoms' movements as a function of temperature, it is possible to extract quantitative values for the activation energy of surface diffusion and atomic vibrational frequencies. The experimental values of the activation energy barriers are not only an essential input in the growth models, but also help to explain the atomic bindings on crystal surfaces. In the investigations of the single atom diffusion processes, the binding energies or the interaction energies between atoms in the atom-atom interactions or the atom-defect interactions gives us an insight on how different atoms on the surface act together with each other. The information obtained will then give us a more general picture in our way leading to the full idea of surface morphology structure.

## 1.4.1 Data Analysis

### 1.4.1.1 Unrestricted random walk

In the way of getting the general picture we need to ask two questions; how do atoms move on a crystal surface, and, at what rate are they moving with. In order to answer both questions we need to have some sort of a formula so we can deal with the ideas of surface transportation. Let's look at the question of the rate of movement first.

From a single atom diffusion system, for an isolated atom migrating on a semi-infinite crystal terrace, we define a relevant diffusion coefficient,  $D$ , as the tracer diffusion coefficient, by

$$2mD\tau = \langle |r(\tau) - r(0)|^2 \rangle, \quad (1.1)$$

where  $m$  is the dimensionality of the diffusion (either 1 or 2 for surface diffusion)\*,  $\tau$  is the time interval of the observation, and  $r$  is the vector position of the adatom. The brackets indicate a time average over repeated observation periods of duration  $\tau$ . By defining  $r(0)$  in Eq.(1.1) as the origin, the diffusion coefficient becomes simply

$$D = \langle r^2 \rangle / 2m\tau, \quad (1.2)$$

where  $\langle r^2 \rangle$  is the adatom's average mean-square displacement during the time interval  $\tau$ . In one dimension,  $\langle r^2 \rangle = \langle x^2 \rangle$  and in two dimensions  $\langle r^2 \rangle = \langle x^2 \rangle + \langle y^2 \rangle$ . From random-walk theory, the mean-square displacement is given by the number of jumps,  $N$ , made by the adatom multiplied by the square of the jump distance,  $l$ , or

$$\langle r^2 \rangle = Nl^2. \quad (1.3)$$

For migration exclusively by thermal activation across a surface with a periodic potential energy distribution, the average number of jumps in a time interval,  $\tau$ , can be written as the product of an attempt frequency,  $\nu_0$ , and a Boltzmann factor or

$$N = \nu_0\tau \exp(-\Delta G/k_B T), \quad (1.4)$$

where  $\Delta G$  is the difference in the Gibbs free energy between the maximum(saddle point) and the minimum(equilibrium site) of the potential energy curve (also called the potential energy well),  $k_B$  is the Boltzmann's constant, and  $T$  is the temperature.

\*From Eq. (1.2), for diffusion in two dimensions the equation will become  $\langle r^2 \rangle / 4\tau$ , or  $\langle r^2 \rangle / 2\tau$  for the diffusion in one dimensions. We will be referring to two dimensions throughout this text.

The Gibbs free energy is usually expressed as a sum of an activation energy of surface diffusion,  $E_d$ , and an activation entropy,  $-T\Delta S$ , so the average number of jumps can be written as

$$N = \nu_0 \tau \exp(\Delta S / k_B) \exp(-E_d / k_B T). \quad (1.5)$$

From Eqs.(1.3) and (1.5) the mean-square displacement is given by

$$\langle r^2 \rangle = \nu_0 l^2 \tau \exp(\Delta S / k_B) \exp(-E_d / k_B T), \quad (1.6)$$

and from Eqs. (1.2) and (1.6) we can then derive an expression for the diffusion coefficient as

$$D = D_0 \exp(-E_d / k_B T), \quad (1.7)$$

where  $D_0$  is all the prefactor terms combined, and is expressed as

$$D_0 = (\nu_0 l^2 / 2m) \exp(\Delta S / k_B). \quad (1.8)$$

In most cases the entropy difference between the saddle point and the equilibrium site is negligible and the prefactor is simply the product of the attempt frequency and the square of the jump distance. If one assumes that the attempt frequency is of the same order as atomic vibrational frequencies ( $\sim 10^{12} \text{ s}^{-1}$ ) and that the jump distance corresponds to the typical nearest-neighbor lattice separations ( $\sim 3\text{\AA}$ ), then  $D_0$  should be roughly  $10^{-3} \text{ cm}^2 / \text{s}$ .

The diffusion coefficient  $D$  has often being referred to as the hopping rate (or the jumping rate), as this will also be referred in the remainder of the text.

### 1.4.1.2 Arrhenius relations

The procedure used to obtain the diffusion parameters is to measure the mean-square displacement at several temperatures and make an Arrhenius plot from Eq. (1.7) of the hopping rate (diffusion coefficient)  $D$  versus the inverse temperature  $1/kT$ . This equation is known as the Arrhenius relation. From a system at equilibrium, an atom spends most of its time vibrating around an equilibrium site in the potential energy well. If we consider an equilibrium site as state A and a next neighbor site as state B, for the atom to move from state A to state B requires the atom to overcome an energy barrier, the so called activation barrier (or the diffusion barrier). And so, this activation energy is the energy needed for the atom to overcome the barrier and causes the system to move from A to B. See Fig 1.11.

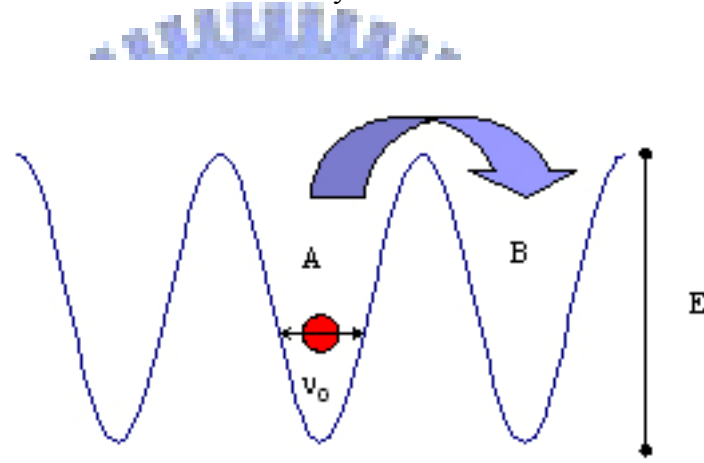


Fig. 1.11 A diagram showing the activation barrier with an atom vibrating at an attempt frequency  $\nu_0$  inside a quantum well. The atom requires an energy  $E$  to overcome the barrier and move from state A to state B.

The hopping rate is the rate at which the atom “jumps” to the neighboring sites (from A to B) at a unit time, usually in seconds. If we take the logarithm of Eq. (1.7), we will obtain an expression as

$$\ln D = -\frac{E_d}{k_B T} + \ln D_0, \quad (1.9)$$

so slope of the plot from the relation in Eq. (1.9) will results in a straight line as  $E_d$ , the activation (diffusion) energy, and the frequency prefactor is the intercept  $\ln D_0$ . Figure 1.12 shows an example of the Arrhenius plot in a case of a Pt atom diffusing on Pt(100) surface [4]. With rates taken at different temperatures it is plotted in a least square fit. The slope and the intercept of the plotted line then yield an activation energy and a prefactor of  $0.47\text{eV}$  and  $1.3 \times 10^{-3} \text{ cm}^2 / \text{s}$ , of the surface diffusion, respectively.

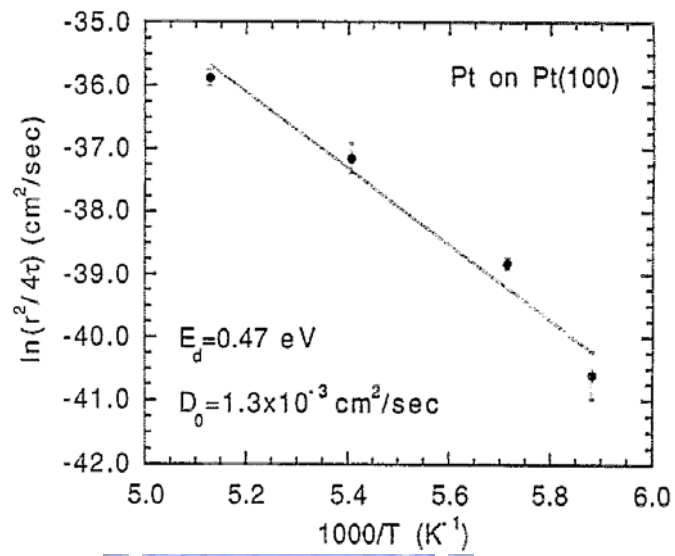
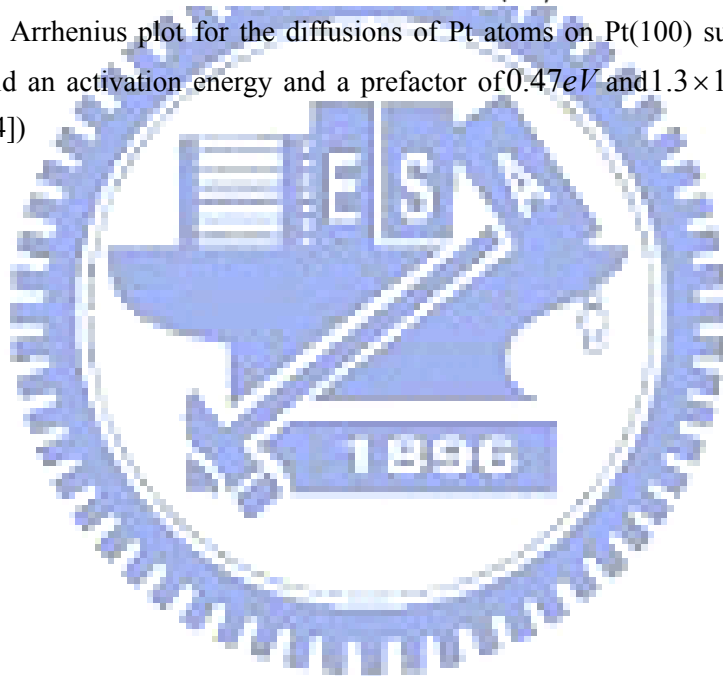


Fig. 1.12 An Arrhenius plot for the diffusions of Pt atoms on Pt(100) surface. The slope and the intercept yield an activation energy and a prefactor of  $0.47\text{ eV}$  and  $1.3 \times 10^{-3} \text{ cm}^2 / \text{s}$  respectively. (From Ref. [4])





### 1.4.1.3 Jump length distributions

Until now, in all previous discussions on diffusion analysis, assumes the displacements take place in single jumps, that is, jumps between adjacent binding sites. It is possible, however, that an atom once promoted to a transition state, can move at distances more than one lattice spacing before retrapping. For diffusions in one dimension, if say, the rate of single jumps is  $\alpha$ , and the rate of double jumps is  $\beta$ , then the probability  $p(x,t)$  of a particle being found at a distance  $x$  from the origin after time  $t$  is given by

$$p(x,t) = \exp[-2(\alpha + \beta)] \sum I_j(2t\beta) I_{x-2j}(2t\alpha), \quad (1.10)$$

where the summation extends over all integer values of  $j$  and  $I_x$  is the modified Bessel function of order  $x$ . Calculations of this probability in comparison to the experimental measured displacement distributions have been done in several adsorbate-substrate systems. The results have indicated that the relative fraction of long jumps is system-specific. Wang et al. [5] find that only nearest-neighbor jumps occur for Re and Mo atoms diffusing on the W(211) surface over a range of temperature studied, whereas for Ir and Rh atoms, a small fraction of the displacements (<5%) are due to long jumps on the same surface. Reports by Lovisa and Ehrlich [6] suggested that long jumps on the W(110) surface occur significantly more often, presumably due to its smaller corrugation. For example, the fraction of long jumps in the diffusion of Ir on the W(110) surface may be as high as 20% [6]. The distribution of the jump lengths is found to be temperature-dependent suggesting that the transition state varies as a function of temperature. It is known that long jumps are more likely to occur at high temperatures where distribution of  $k_B T$  is comparable to the activation barrier for diffusion. At lower temperatures, long jumps are thought to occur if the energy dissipation to the substrate lattice is weak [7]. If one ignores the presence of long jumps, for most systems, it may introduce a source of error in measuring the activation energy. Long jumps have a strong contribution to the determination of the activation barrier from measurements of diffusing atoms [8].

## 1.4.2 Transport Mechanisms

After we answered the question on the rate of moving atoms, we will now focus on the way atoms move on a crystal surface. With intensive studies on the morphological evolutions of the atoms roaming around on surfaces, new basic mechanisms are still being proposed and discovered. The competing roles of the interstitials and the vacancies with their relative magnitudes are being established across a wide range of materials. There are three basic types of transport mechanism established. They are the hopping (or jumping) mechanism, vacancy-mediated diffusion mechanism, and the exchange mechanism.

### 1.4.2.1 Hopping mechanism

Single atoms were long to be thought of diffusing on surfaces by simply jumping from site to site, see Fig. 1.13. The atom in the figure hops over a neighboring atom from its original adsorption site to the next by overcoming the activation energy barrier. This classical view of surface diffusion has been somehow proved to be too simple and doesn't give enough explanations to the whole picture. The situation is considerably more complicated than atoms simply hopping around. With the development of microscopic techniques now we are able to study the surfaces at the atomic scale, and even tracking single atoms along their diffusion paths. This has indeed given us more information in understanding the evolution of surface morphologies with the growth model.

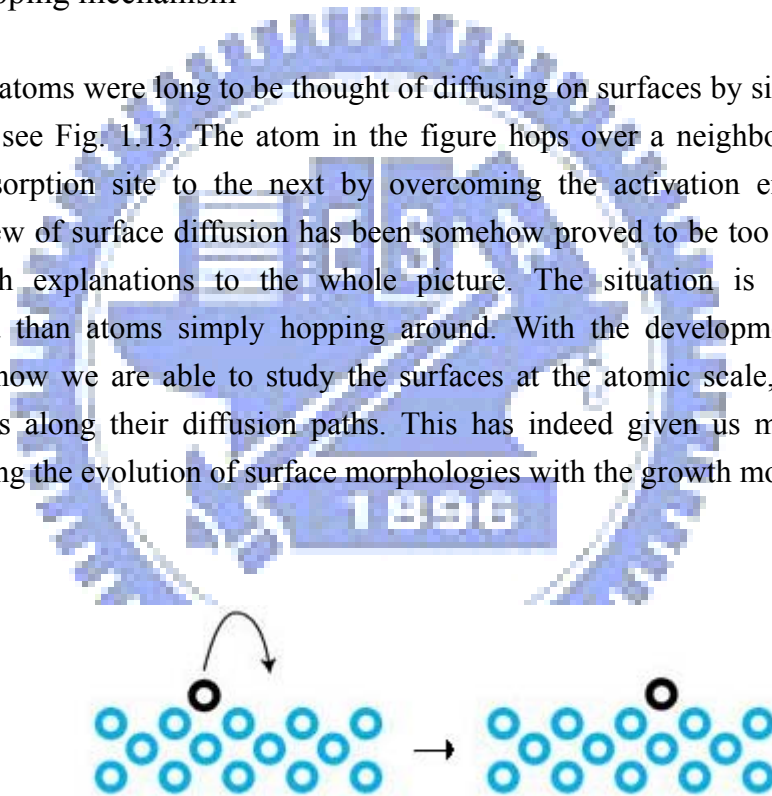


Fig. 1.13 A simple schematic diagram showing the hopping mechanism, in which an atom hops over a near by atom from one adsorption site to the other neighboring preferential site.

#### 1.4.2.2 Vacancy-mediated diffusion mechanism

Vacancy has been invoked in the past to explain the incorporation of foreign atoms into a surface. The vacancy-mediated diffusion mechanism of embedded atoms was first proposed for the motion of Mn atoms in Cu(001) during the formation of a surface alloy [9]. As vacancy defects tend to increase as temperature increases, one would expect vacancies to play a dominant role in surface diffusion. An easier way of visualizing this is by imagine there is a simple two-dimensional slide-tile game with a single missing tile (vacancy), one need to push the tile (atom) to fill the empty tile (vacancy) space in order to bring the randomly disordered tiles back into order. In doing so, it looked like that vacancy is moving on the surface, but in reality, it is the atom that is doing the work. On some surfaces, vacancy diffusion can be very significant. Figure 1.14 gives an idea of the diffusion event with surface vacancy displacements.

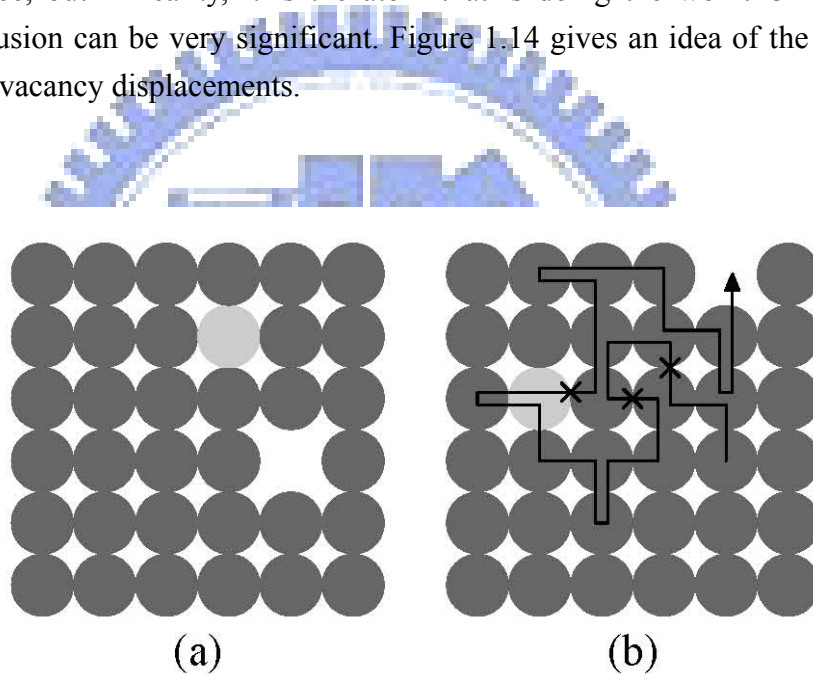


Fig. 1.14 A schematic diagram showing a diffusion event of a surface vacancy. The arrow indicates a random pathway of the vacancy as it diffuses from the original site, as shown in (a), to the final position, as shown in (b). The atom-vacancy exchanges are marked with the crosses to show the pathway of the bright atom between its starting and end points. (Adopted from Ref. [12])

### 1.4.2.3 Exchange mechanism

Exchange mechanism has important implications in the fabrication of artificially layered structures. For that reason this mechanism has attracted a lot of interest in establishing the conditions that determine whether ordinary hopping or a particular exchange mechanism should be preferred. In 1990, Kellogg and Feibelman proposed a very different mechanism for surface diffusion [10]. They reported with an idea of an atom adsorbed on top of a crystal surface, instead of hopping from site to site, moves by pushing its way into the first layer of the surface and popping the atom that is in its way out onto the surface (Fig. 1.15). This “exposed” atom on the surface then moves into other preferred site and reinsert itself into the first layer of the surface. Since atoms all look alike and is difficult to distinguish one from the other, it looks as if the atom has jumped from one place to another. But what really happened is that the atoms on and in the surface have swapped places, skipping a lattice site in the process. Theoretical research has reported that the energy barrier for the place-exchange diffusion is lower than hopping diffusions by several tenths of an eV. Sometimes this mechanism is the more preferred one than the other in terms of the energy needed in atom excitation.

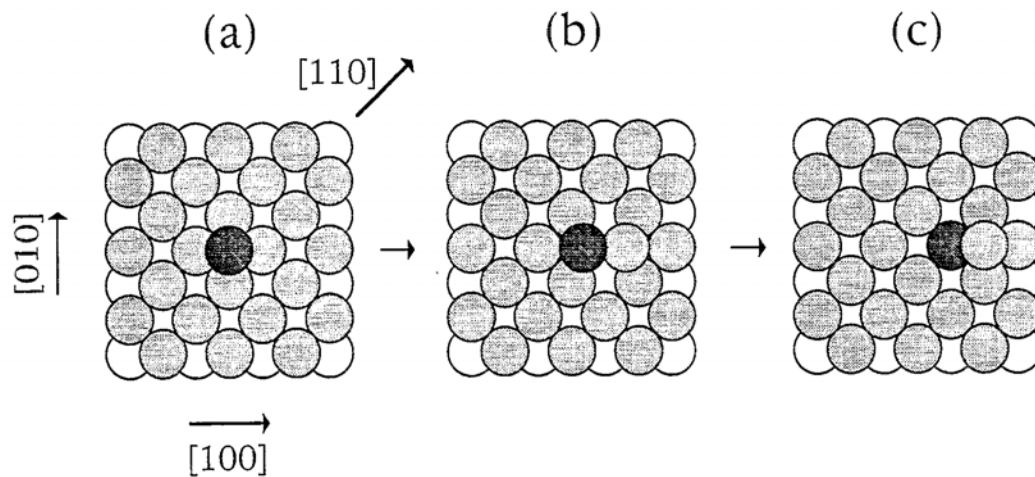


Fig.

1.15 A schematic representation of the exchange mechanism on a fcc(100) surface. (a) A dark atom resides at a four-fold hollow site changes places with the neighboring substrate atom by inserting itself into the layer while the substrate atom moves up in a concerted motion. (b) The two atoms are now in equivalent positions with a vacancy below. (c) The dark atom then fills the vacancy space while the displaced substrate atom now becomes the new adatom on the surface. (Adopted from Ref. [21])

## 1.5 Literature Reviews

From the past studies in the field of individual atoms migrating across single crystal terraces and their incorporation into the top layer of surface atoms have shown that the adsorbed atoms or molecules can be used to change the surface morphologies of thin-film growth for specific material applications. So, it is very important and also very interesting to find out the roles a given adsorbate will play in the growth process with modifications.

### 1.5.1 Cl-terminated Si(100)-(2x1) surface

The main properties of the Si(100)-(2x1) surface obtained from scanning tunneling microscopy (STM) has been widely studied. Single-atom diffusions on the (100) crystal planes is an excellent model system for investigation of the adsorbate mediated surface diffusions and the atom incorporation processes. By studying surface diffusions on the (100) surfaces, one can derive information on how adsorbate affect both the rate of surface diffusion as well as the energy barrier for incorporation of adatoms into the surface layer.

It is known that the top layer atoms of the Si(100) surface reconstruct to form parallel rows of dimers, which establish two well-differentiated directions, in parallel and perpendicular to these rows, as shown in Fig. 1.6. By exposing Si(100)-(2x1) surface to chlorine molecules at room temperature, chlorine atoms tends to saturate at the dangling bond sites of the surface. There are five geometrically distinguishable configurations of the arrangement of neighboring pairs of Cl atoms on the Si surface. The most probable like arrangement is the chemisorption of two Cl atoms on the Si dimer sites in adjacent rows, as shown in Fig. 1.16, labeled type III a + III b. The probability of this configuration is 0.52. For type II a and II b, where Cl atoms bonded to the adjacent dimers in the same dimer row, as shown in the same figure, the probability is 0.33. For two Cl atoms to be present on the same Si dimer is the least likely with a probability of 0.15, as labeled type I in Fig 1.16.

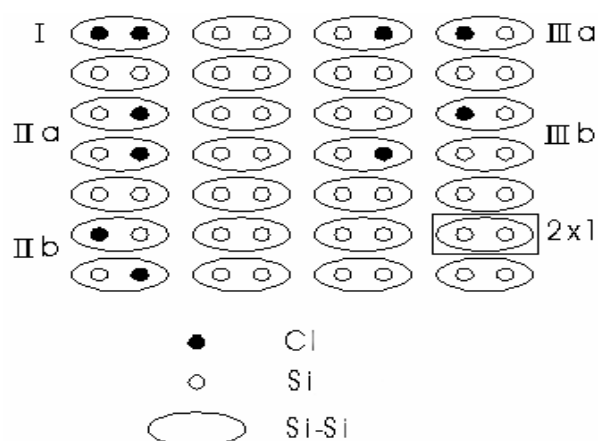


Fig. 1.16 Schematic diagram of the five geometrically distinguishable configurations of the neighboring pairs of Cl atoms on the Si(100)-2x1 surface.

If we increase the exposure of the chlorine gas, the density of the fully Cl-terminated dimers increases. In the end, all the dimers with dangling bonds on the surface will be terminated with chlorine atoms. The adsorption of Cl molecules does not disrupt the sigma bonds, but breaks the weak pi bonds existed on the clean Si(100)-(2x1) surface. Therefore, each dimer has terminated with two Cl atoms, as one Cl per Si, in the Cl-saturated Si(100)-(2x1) surface, now covered with one monolayer of chlorine atoms. This will serve as the base of our experiment. For long we have thought the vacancy defects shown on the surface with the empty sites are just simply the Cl atoms from the monolayer has gone missing from these sites. But after a closer look, some of these empty sites, now called vacancies, are actually moving, with the increase in temperature. It will be interesting to see how these vacancies move, how fast they are moving, and most important of all, the mechanisms behind their movement.

### 1.5.2 Case studies-Vacancy diffusions

Before we move on to the next section about Cl extraction by hydrogen atoms from Cl-saturated Si(100) surface, we need to look at a number of cases to get an idea of the experiment. There have been several studies regarding the structures and kinetics of vacancies on Si surfaces. In 1993, MIT's J. Wang, T. Arias and J. Joannopoulos identified the possible mechanisms contributed to the low formation energy and the stability of dimer vacancies on the Si(100) surface, as: (i) the need to eliminate dangling bonds in the second layer and (ii) the need for atoms to readjust in order to relax the strain [3]. Later in the same year, N. Kitamura *et al.* reported on thermal vacancy diffusions by real-time STM observations on the Si(001)-(2x1) surface where they tracked the motion of single dimer vacancy jumps using a novel method of repeated line scans [19]. They then obtained the activation energy of 1.7eV for the vacancy diffusions through an Arrhenius plot (Fig 1.17). They concluded that the motion of vacancies is predominantly one dimensional along the dimer rows. They also believed that the single dimer vacancy jump is preceded by a place exchange mechanism between the atom pairs from the top and the second layers.

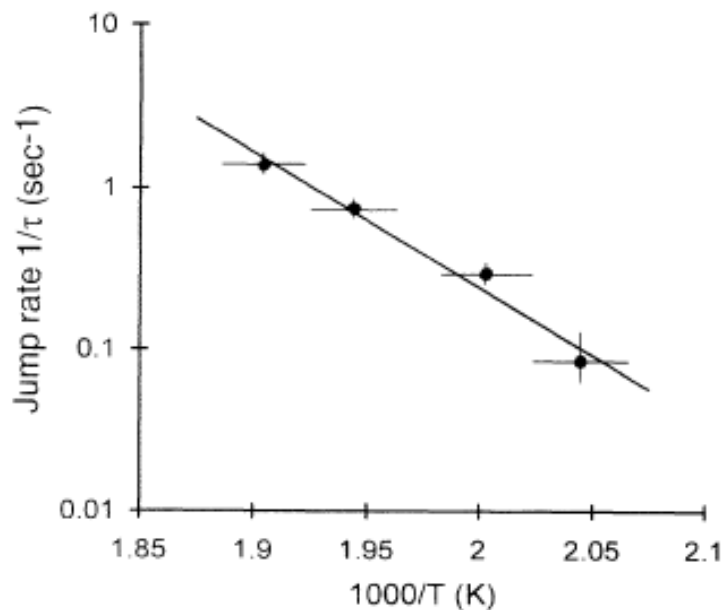


Fig. 1.17 An Arrhenius plot for the single dimer vacancy jump rate. From this plot they obtained an activation energy of 1.7eV. (Ref. [19]).



Vacancy diffusion has also been seen on other material and structures other than Si(100). For example, a recent report on surface diffusion of single vacancies on the Ge(111)-c(2x8) surface by means of variable temperature scanning tunneling microscope is also been observed [10]. The vacancies were deliberately created with the STM at different sample temperatures by slight tip-sample contacts (Fig1.18). They have found that the diffusion of such generated vacancies is a thermally activated motion. The vacancies have higher mobility along the parallel direction to the adatom rows than in the perpendicular direction to them. They found that the activation energy barrier along the rows is slightly lower than the activation energy barrier that is perpendicular to them (0.83eV vs. 0.95eV, respectively). They have also plotted the Arrhenius relation for the diffusion coefficient  $D$  at different temperatures and measured the activation energy  $E_d$  and the prefactor  $D_0$  of the system to be 0.88eV and  $10^{14.3} \text{ s}^{-1}$ , respectively (Fig. 1.19).

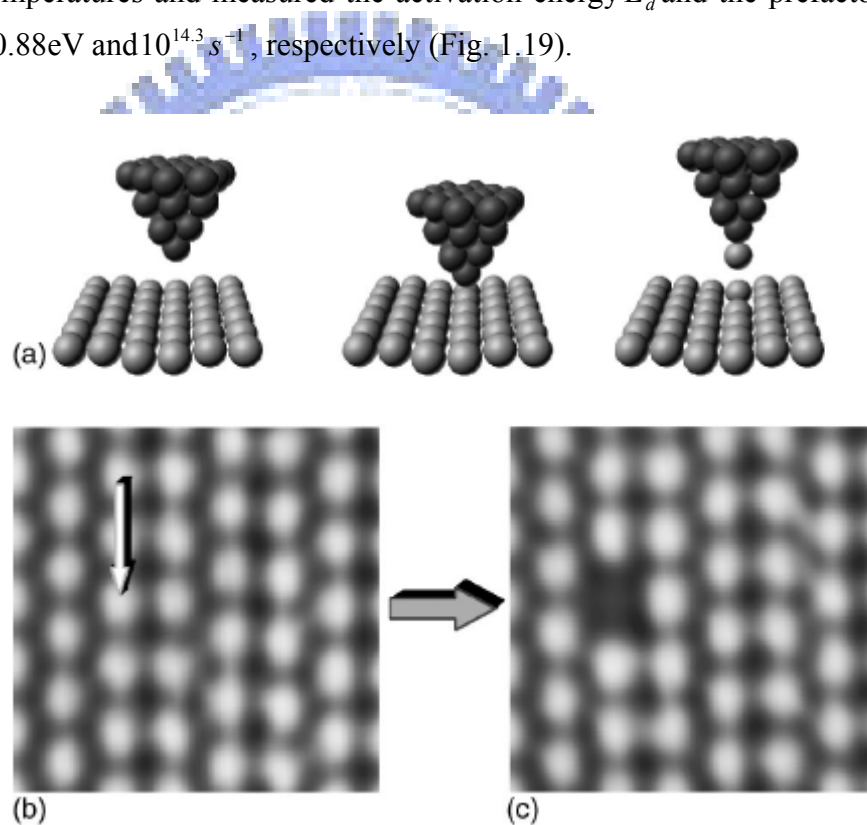


Fig.1.18 (a) Schematic representation of the extraction procedure of a single Ge atom. (b) and (c) are constant current images showing a region before and after the creation of a single vacancy. (Image Adopted from Ref. [10]).



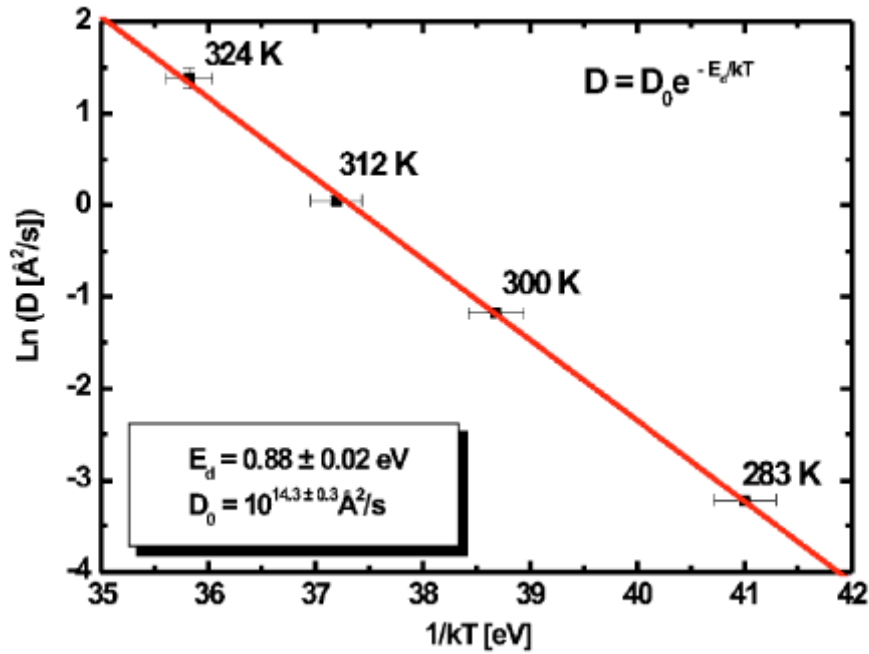


Fig. 1.19 The Arrhenius plot for the diffusion coefficient  $D$  at different temperatures. The measured activation energy and prefactor of the system was  $0.88\text{eV}$  and  $10^{14.3}\text{s}^{-1}$  respectively. (Ref. [10]).

For a more interesting case we will be looking at vacancy diffusions on the Cu(100) surface experiment done by van Gastel *et al.* [11-12] few years back. In the experiment they deposited indium atoms on a clean copper surface. The indium atoms embedded on the outermost atomic layer of the surface, and with the help of STM they traced the particles at room temperature to reveal the mobility of the atoms in the surface. The indium atoms rapidly incorporated in the outermost atomic layer, where each one replaces a single copper atom. They soon discover that the embedded indium atoms are mobile as they actually jumped over multiple lattice spacings, and the jumps were separated by a relatively long intervals of about 100 seconds at room temperature. The neighboring indium atoms also seem to jump simultaneously, causing a concerted motion. These are shown in figure 1.20. In order to explain this unusual behavior of the indium atoms they assumed the motion is assisted by an ‘invisible particle’ that is rapidly diffusing on the surface. This particle will randomly diffuse two-dimensionally on the surface and will have a high chance of bump into the indium atoms several times, thereby making the In atoms being displaced at a distance of more than one lattice spacing in a time too short to be observed by STM. This long jump could also happen to other indium atoms simultaneously due to its fast movement.

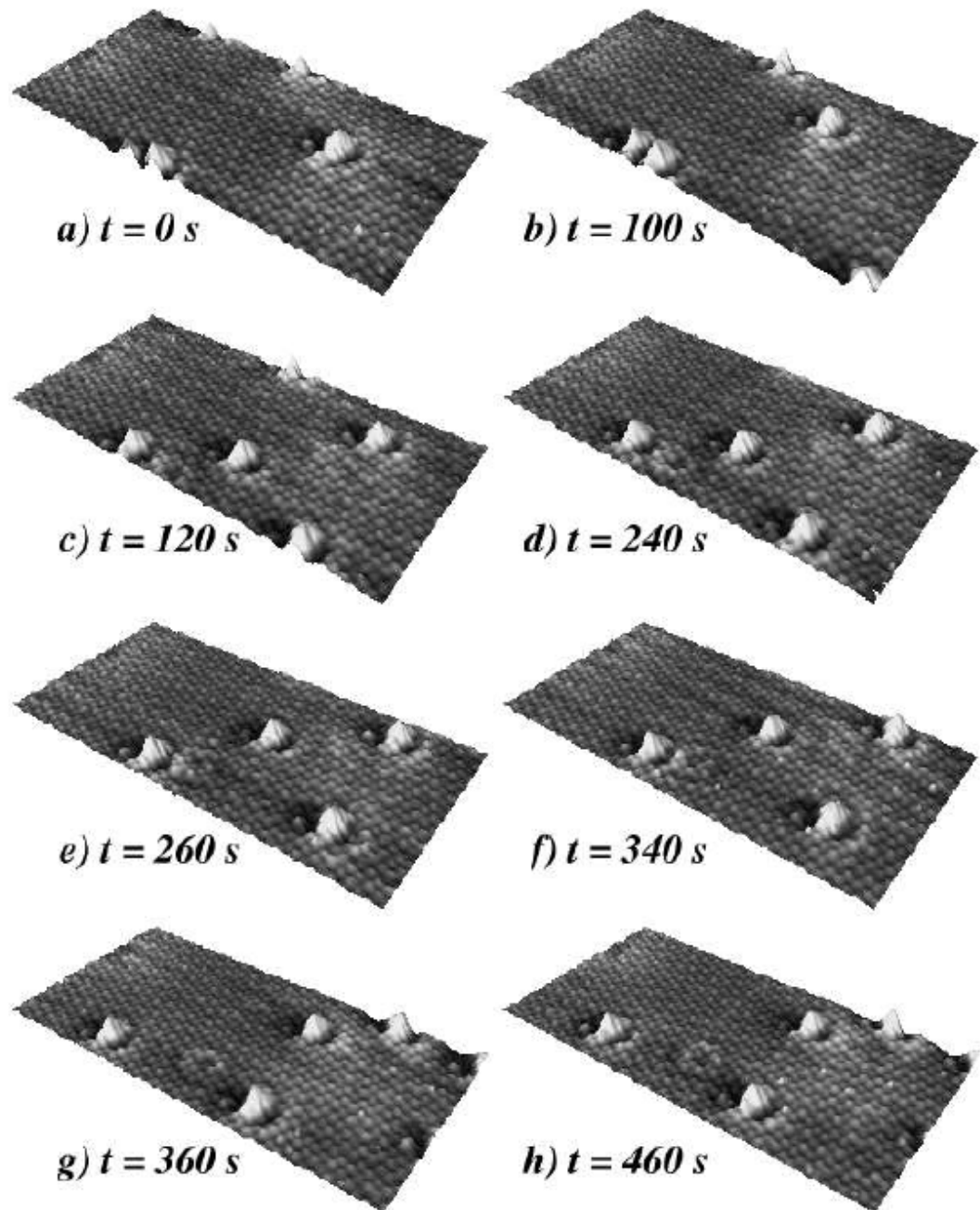


Fig. 1.20 STM images of the Cu(001) surface at room temperature illustrating the diffusions of the embedded indium atoms. Image (a) shows five of the embedded indium atoms. Image (b) shows after 100 s the indium atoms remained in position. In the next image (c) all the indium atoms have made a multi-lattice-spacing jump. After this jump, the indium atoms again stayed at the same position as shown in the image (d) for a further of 2 minutes. From images (e)-(h) it shows that this pattern of long jumps separated by long time intervals repeats itself. (Images Adopted from Ref. [12]).

There could be three possibilities responsible for the assisting role, namely an adsorbed residual gas molecule, single copper atoms on top of the surface, and the vacancies. In the case of diffusions of an embedded indium atom assisted by an adsorbed molecule from the residual gas in the vacuum system, the rate of the long jump would not agree with the rate of the adsorption of the gas molecules should it depends on it. The length of the long jump also depends on the residence time of the gas molecules residing at the indium atoms, in which the time of residence of the molecules goes down exponentially with temperature, so the jump length of the In atoms should do the same. Lastly, after desorption of the residual gas molecule, it should no longer be present on the surface and is therefore not available to assist the indium atoms in making the long jumps. The case with the exchange of the copper atoms, most indium atoms, immediately after the desorption on top of the surface, stays close to the steps rather than inserting themselves into the first copper layer, resulting a homogeneous population of the terraces with indium. This thus rules out the possibility and they concluded that surface vacancies are the ones responsible for the diffusions on the Cu(001) surface with indium atoms. They also concluded that the reason why one can not 'see' the vacancies is because the probability for even a single vacancy to be present in the scanning area is very low, and the rate at which each vacancy moves is much higher than the imaging rate of the STM. The short range attraction between the indium atom and the vacancy makes the jump length of the indium atom somewhat larger than that of the copper atoms. The distribution of the waiting times between successive jumps is purely exponential, which shows that subsequent (long) jumps are the effect of the passage of different vacancies. Vacancy diffusion mechanism is the main transport mechanism on the surface with measured activation energy of 0.699eV and a frequency prefactor of  $10^{10.4} \text{ Hz}$  (Fig. 1.21).

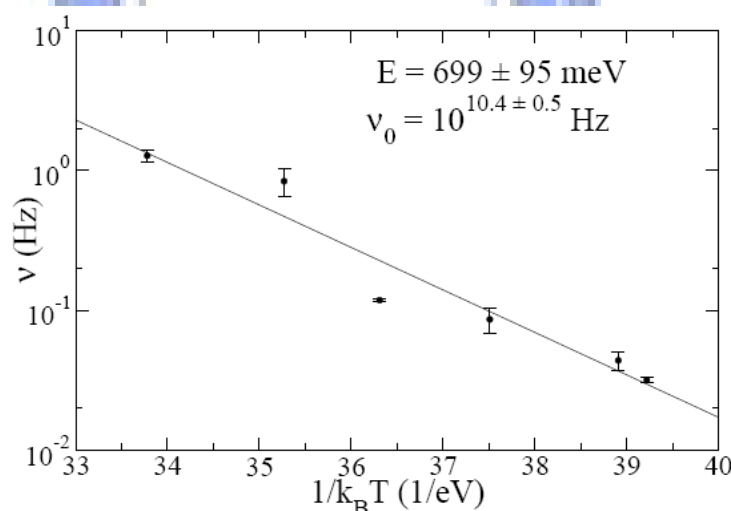


Fig. 1.21 Arrhenius plot of the long jump rates of the embedded indium atoms. The activation energy and the prefactor calculated were 0.699eV and  $10^{10.4} \text{ Hz}$  respectively. (Ref. [12]).

### 1.5.3 Enhancement of surface diffusion with adsorbed H

Hydrogen is a common adsorbate used in a variety of surface science studies and is a good choice for the modification of the morphology of the epitaxial films and their growth on both metal and semiconductor surfaces [13]. Adsorption of hydrogen can alter the surface properties such as the surface energy, the adatom diffusion, and the nucleation processes. There have been reports discussing about the enhanced mobility of adatom diffusions and defect formation on hydrogen adsorbed surfaces. In which the migration of the adatoms is assisted by the mobility of hydrogen atoms. For example, investigation on a Be surface with hydrogen atoms adsorbed at the defect sites has been reported [14]. It has said that adsorbed H atom reduces the activation barrier and the formation energies for the surface defects. It reduces the surface atom diffusion barriers by a factor of 3. Hence, helps the diffusion process. This is also seen in other numerous reports, all with the influence of gas adsorbates, typically hydrogen, on the diffusion of adatoms on metal and semiconductor surfaces [15-17]. Therefore, hydrogen could be used to control the thin-film growth at the atomic level.

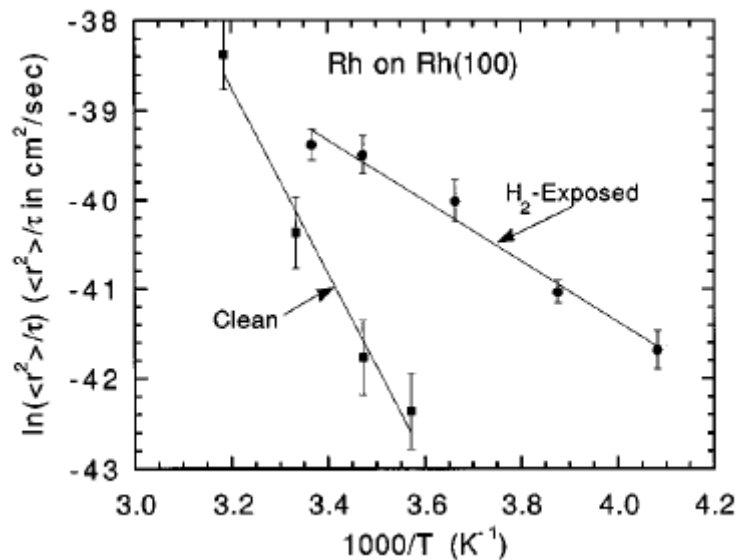


Fig 1.22 Arrhenius plot with temperature dependence of the mean-square displacement for self-diffusion on Rh(100) for the clean and the hydrogen-exposed surfaces. From the plot, it shows clearly that the presence of hydrogen leads to a large reduction in the activation energy and the corresponding prefactor. (Ref. [15]).

#### 1.5.4 Cl extraction by H-atoms from Cl-terminated Si(100) surface

As mentioned, the Cl-terminated Si(100)-(2x1) surface is made up of dimer rows in which Cl atoms saturated on the dangling bond sites forming Si-Cl covalent bond dimers. From an earlier report on the investigation of the relative topic done in our laboratory, we investigated about the correlation of reaction sites in the Cl-terminated Si(100) surface where Cl absorbents were extracted by hydrogen gas atoms [18]. From the system, an incident H-atom flux would react with the Cl atoms that are adsorbed on the Si(100) surface. Together they form gaseous HCl molecules, as:  $H + Cl / Si(100) \rightarrow HCl + Si(100)$ . This gas-surface reaction will reduce the number of chlorine atoms on the Si surface at low temperatures and hence creating a number of vacancies along the first layer of the surface, as shown in figure 1.23. The dark sites in the figure are the H-terminated sites.

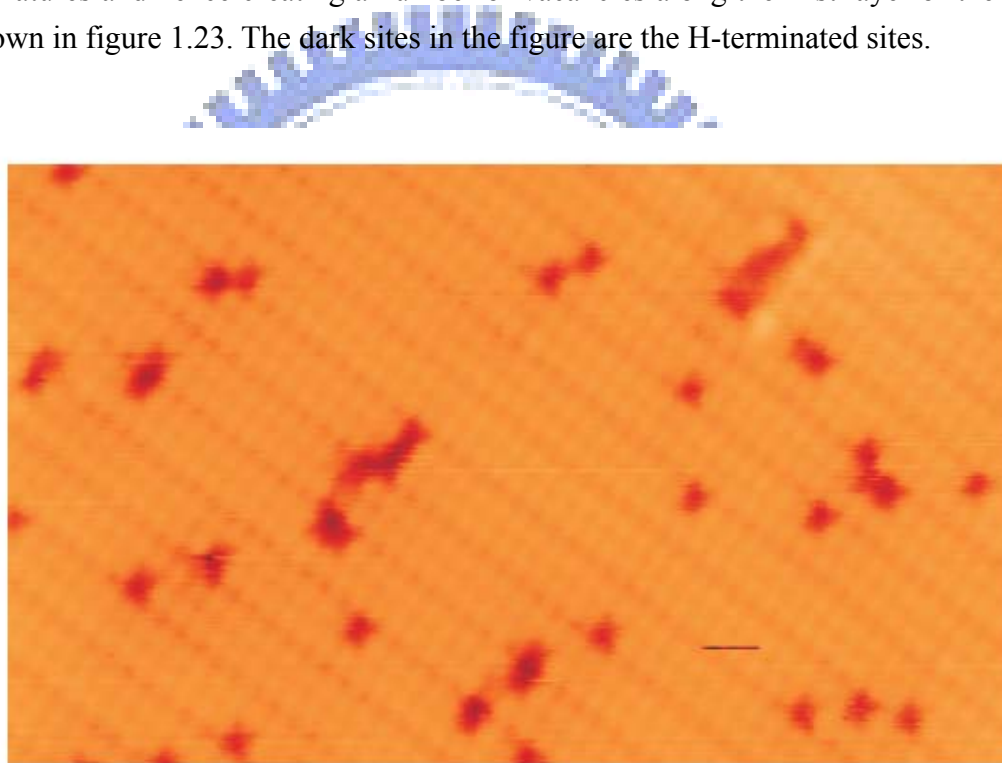


Fig. 1.23 A STM image of the Cl/Si(100)-(2x1) surface after 12 L apparent dosages of H atoms at a sample temperature of 600 K. The dark sites in the image are the H-terminated sites. The sample bias used was +2 V. (Image Adopted from Ref. [18]).

These newly created vacant dangling bond sites caused by the removal of Cl atoms in the Si-Cl dimers exhibit a higher apparent height due to enhanced tunneling near the Fermi level and are highly reactive. It is now easier to tunnel into or out of these bond sites. Hydrogen atoms may be energetically favorable to adsorb on either end of the dimers, and so these vacancy sites are then been filled again by succeeding hydrogen atoms in a continuous dosage of gaseous hydrogen. Hydrogen atoms form a strong Si-H covalent bond with the silicon atoms from the second layer of the surface and most of them are isolated by neighboring chlorine atoms. The Cl-extracted sites by impinging H atoms are randomly distributed, and the density of the Cl-extracted sites increases as the dosage of the H atoms becomes higher, as seen in the sequential STM images in figure 1.24.





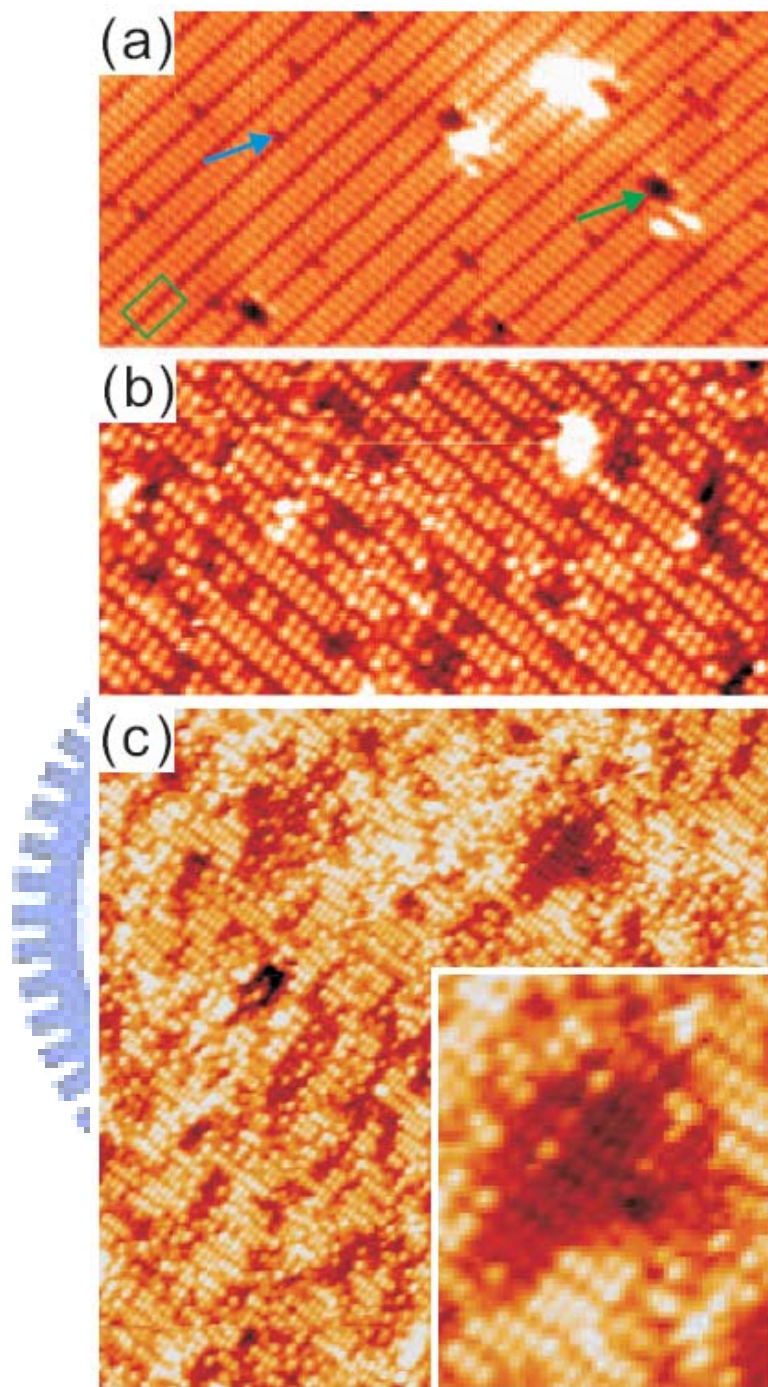


Fig. 1.24 STM images of the Cl/Si(100)-(2x1) surface after (a) 0, (b) 36, and (c) 90 L apparent dosages of H atoms. The sample bias used was +2 V. In (a) the green rectangle box, running from the upper right to the lower left, encloses a row of five Cl-Si-Si-Cl (monochloride) species. A surface Cl atom appears as a bright protrusion and forms a narrow ellipse with another in the neighboring monochloride row in the image. The green and blue arrows point to a missing dimer defect site and a H-termination site, respectively. The inset in (c) shows a 2x1 area of nearly complete H-termination after Cl-extraction. Clearly the density of the Cl-extracted sites increases as the H-atom dosage increases too. (Images Adopted from Ref. [18]).

A high-resolution core-level photoemission spectroscopy is useful to distinguish the atoms at nonequivalent sites and in different chemical bonding configurations, according to the shifts of their binding energies. Following is a figure showing the respective surface-sensitive Cl 2*p*, Fig. 1.25 (a), and Si 2*p*, Fig. 1.25 (b), core-level spectra, and their decomposition into constituent components from the Cl-Si(100)-(2x1) surface before and after H bombardment at 325 K for various dosage.

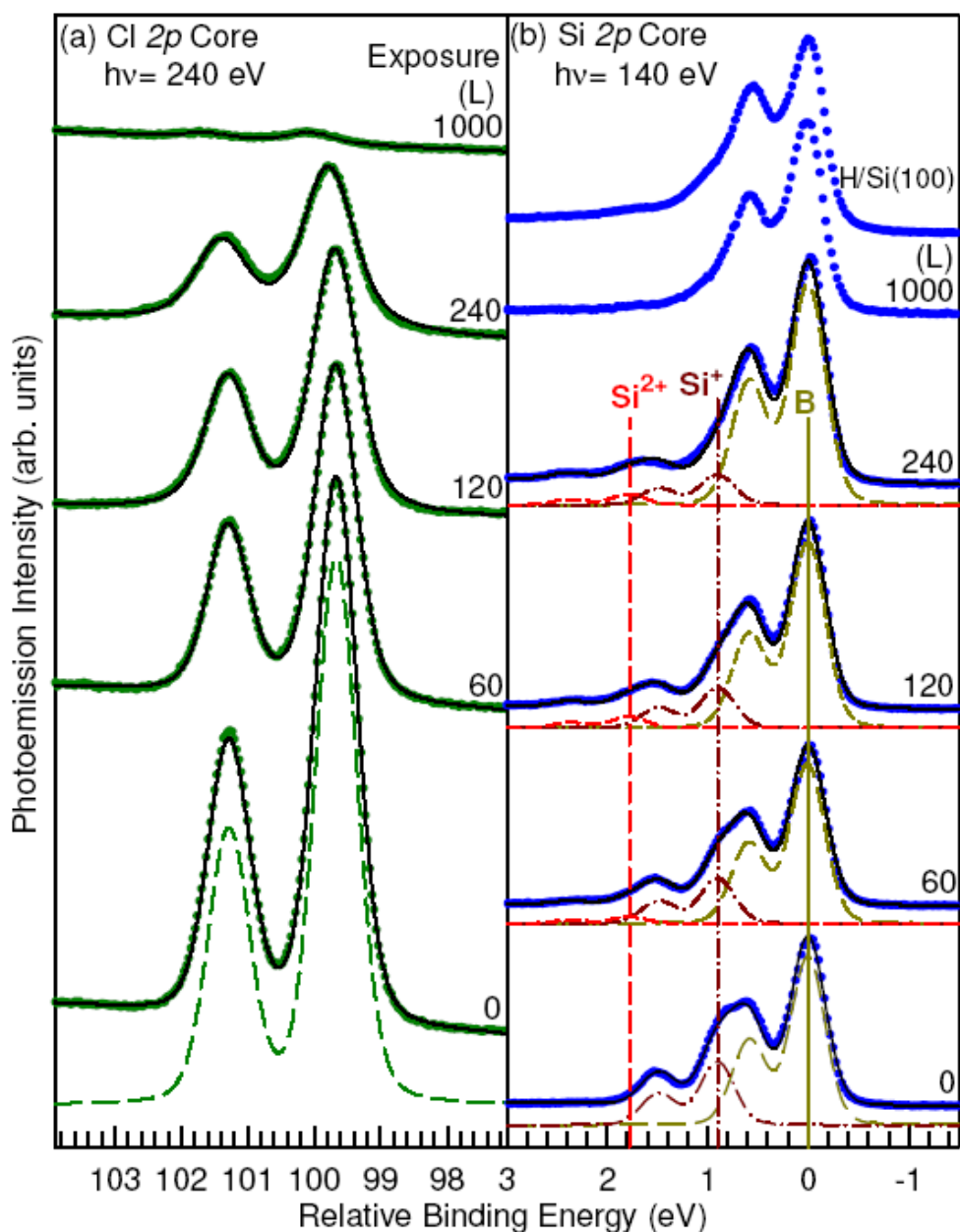


Fig. 1.25 The (a) Cl 2*p* and (b) Si 2*p* core level photoemission spectra for the Cl-Si(100)-(2x1) surface with the same surface after various apparent H-atom dosages as labeled. The solid curves are fits to the spectra. (Ref. [18]).



## Chapter 2 Experiment Setup

### 2.1 The Vacuum System

Scanning tunneling microscopy (STM) experiments was conducted in an ultrahigh-vacuum (UHV) system. The main chamber is equipped with a VT-STM (Omicron), a manipulator, a pumping system, and gas sources, including  $H_2$ ,  $Cl_2$  and  $G_2H_6$ , as shown in Fig. 2.1. The pumping system is consisting of a dry pump, a turbo pump, a titanium sublimation pump (TSP), and an ion pump. The base pressure of this vacuum system is about  $2 \times 10^{-10}$  torr.

We first use the dry pump to lower the pressure in the vacuum chamber to  $\sim 10^{-3}$  torr. The turbo pump then automatically starts to lower the pressure to a range of about  $10^{-6}$  torr. It is at this low pressure, the ion pump is then turned on. The main chamber is parted into three sub-chambers; a loading chamber, a preparative chamber, and an observation chamber, as shown in Fig. 2.2. As the pressure drops to  $\sim 10^{-7}$  torr, we then heat the loading chamber up to a temperature about  $120^\circ\text{C}$  for 16~24 hours. The purpose of this step was to separate the gas and the moisture inside the loading chamber since the tip and the samples were placed in this chamber. After we let the chamber to cool down to room temperature, we then transport the tip and samples to the preparative chamber where it was held before the actual experiment event. In this, now we have gained the ultra-high vacuum state with a pressure of about  $2 \times 10^{-10}$  torr. Finally, the experiment was conducted in the observation chamber where samples are been observed and measured using the scanning tunneling microscope.

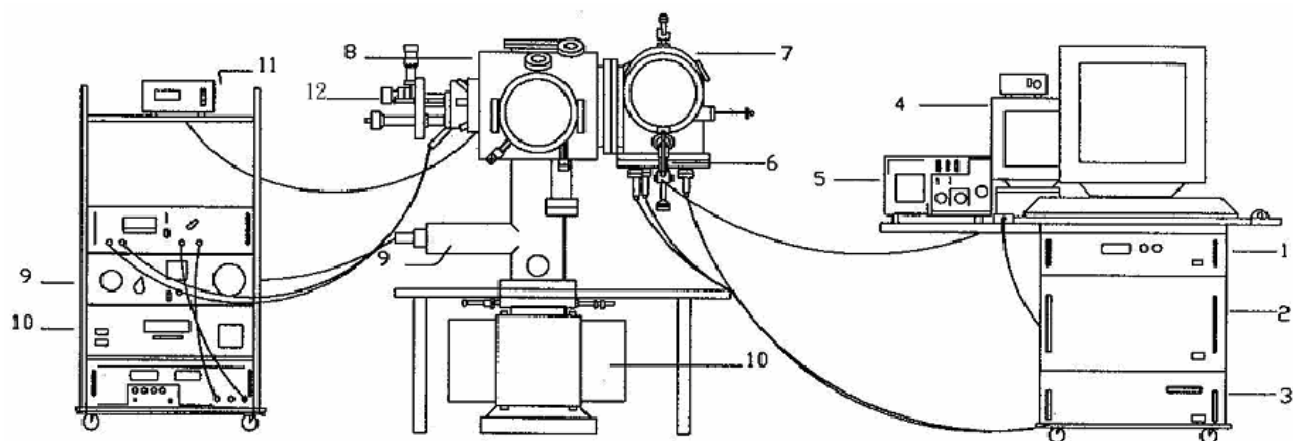


Fig. 2.1 The side view of the STM system. 1. STM variable temperature controller; 2. STM hardware controller; 3. STM work station; 4. CCD camera monitor; 5. Oscilloscope; 6. CCD camera; 7. STM chamber; 8. Main chamber; 9. TSP and TSP controller; 10. Ion pump and ion pump controller; 11. Ion gauge; 12. Manipulator (adapted from Perng-Horng Wu, 1997).

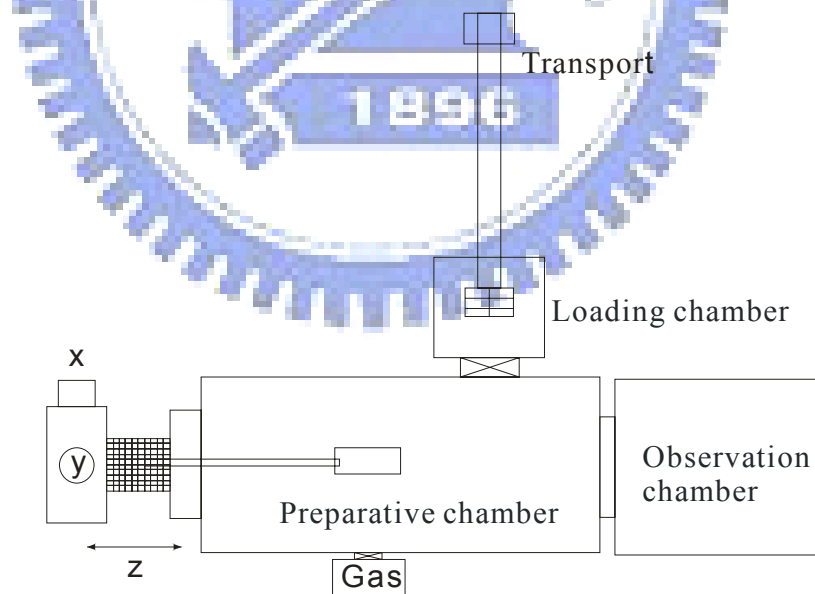
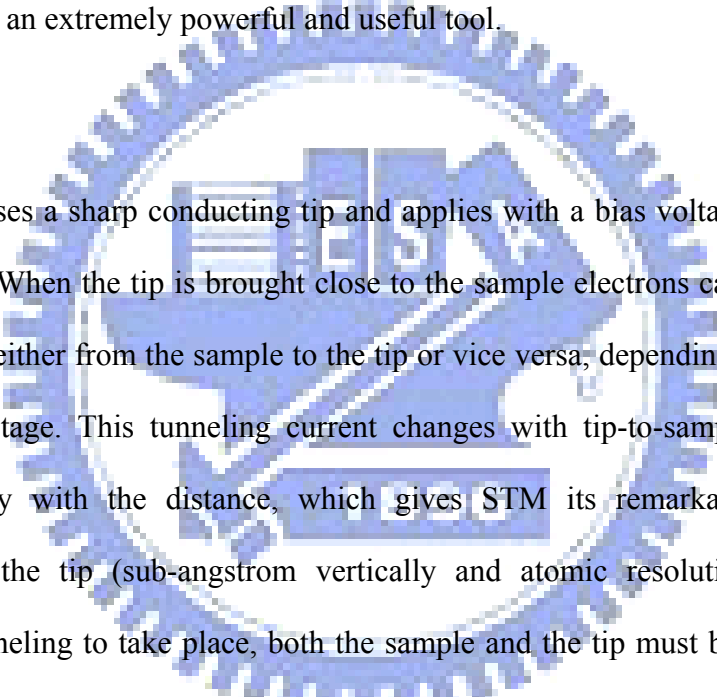


Fig. 2.2 Two-dimensional diagram that illustrates the chamber consisting of loading chamber, preparative chamber, and observation chamber.

## 2.2 Scanning Tunneling Microscope (STM)

### 2.2.1 An introduction

In 1981, G. Binnig and H. Rohrer Invented STM and obtained the first successful operation with atomic resolution using the system the following year. Since then, STM technique has been widely used in various applications and fields. For example, it was used mostly in the fields such as condensed-matter physics, chemical and biological physics, and etc. Especially after it has resolved the Si(111)-(7x7) structure in real space, STM was then proved to be an extremely powerful and useful tool.



STM uses a sharp conducting tip and applies with a bias voltage between the tip and the sample. When the tip is brought close to the sample electrons can "tunnel" through the narrow gap either from the sample to the tip or vice versa, depending upon the induction of the bias voltage. This tunneling current changes with tip-to-sample distance, it decays exponentially with the distance, which gives STM its remarkably high precision in positioning the tip (sub-angstrom vertically and atomic resolution laterally). For the electron tunneling to take place, both the sample and the tip must be conductive, and thus STM cannot be used on insulating materials. Figure 2.3 shows a diagram with the essential elements of an STM. A detailed explanation will follow that.

### 2.2.2 The STM system

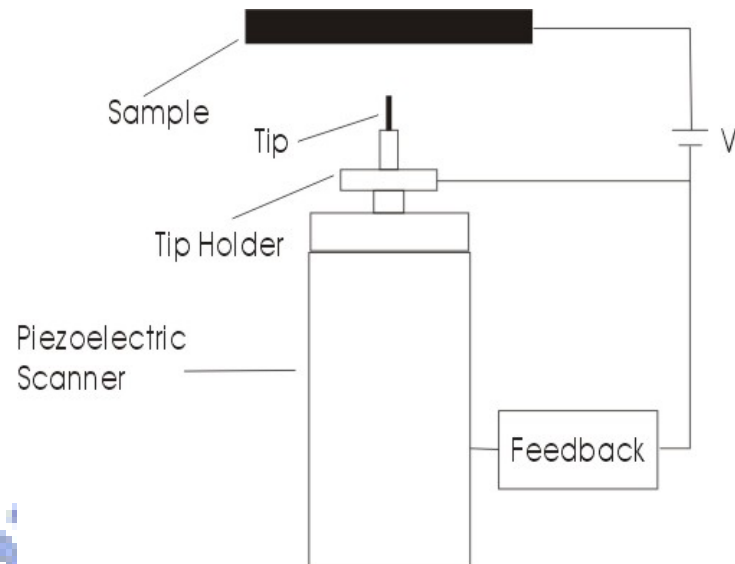


Fig. 2.3 A schematic diagram showing the essential elements of STM.

As shown in figure 2.3, a probe tip, usually made of tungsten (W) or Pt-Ir alloy, is attached to a piezoelectric scanner. By using the coarse positioner and the z-piezo, the tip and the sample are then brought to a distance within a few angstroms of each other. A bias voltage, applied between the tip and the sample, causes an electrical current to flow. This is a quantum-mechanical phenomenon, tunneling, which is the principle theory of the scanning tunneling microscopy. To achieve atomic resolution, vibration isolation is essential. A commonly used vibration isolation system consists of a set of suspension springs and a damping mechanism. This will help to reduce the amount of vibrations.

### 2.2.3 Principles of Electron Tunneling

The operating principle of the STM is based on the quantum mechanical phenomenon of tunneling. In this section, we will discuss the concept of the tunneling phenomenon through a one-dimensional model.

From classical mechanics, an electron with energy  $E$  moving in a potential  $U(z)$  can be described by

$$\frac{p_z^2}{2m} + U(z) = E, \quad (2.1)$$

where  $m$  is the electron mass,  $9.1 \times 10^{-28}$  g. In the regions where  $E > U(z)$ , the electron has a nonzero momentum  $P_z$ . It means that the electron has the ability to be in those regions. Whereas in regions with  $E < U(z)$ , electrons cannot penetrate into those regions. In other words, electrons with energy  $E$  will be unlikely to be found in the regions where  $E < U(z)$ . In quantum mechanics, the state of the same electron is described by a wave function  $\Psi(z)$ , which satisfies the Schrödinger's equation, as

$$-\frac{\hbar^2}{2m} \frac{d^2}{dz^2} \Psi(z) + U(z)\Psi(z) = E\Psi(z) \quad (2.2)$$

where  $\Psi(z)$  is the wave function of the electron.

For an electron with  $E = U/2$  incident upon in a square barrier from the left, as shown in Fig. 2.4, the Schrödinger's equation of this electron thus becomes

$$-\frac{\hbar^2}{2m} \frac{d^2}{dz^2} \Psi(z) + \frac{1}{2} U\Psi(z) = 0 \quad (2.3)$$

and it has a solution of

$$\Psi(z) = \begin{cases} Ae^{ikz} + Be^{-ikz} & (z < 0), \\ Ce^{Kz} + De^{-Kz} & (0 < z < s), \\ Fe^{ikz} & (z > s), \end{cases} \quad (2.4)$$

where  $k = \frac{(2mU)^{1/2}}{\hbar}$ ;  $K = \frac{(mU)^{1/2}}{\hbar}$ .

Eq. 2.4. can be solved for the transmission coefficient  $T = |F/A|^2$  by matching of the boundary conditions on  $\Psi$  and  $d\Psi/dz$  at  $x = 0$  and  $x = s$ . That is

$$T = \frac{1}{1 + \left(\frac{k^2 + K^2}{2Kk}\right)^2 \sinh^2 Ks} \quad (2.5)$$

Because the barrier width  $s$  is much thicker than the wave function decay length  $1/K$ ,  $Ks \gg 1$ , the transmission coefficient can then be approximated as

$$T \approx \frac{16k^2 K^2}{(k^2 + K^2)} e^{-2Ks} \quad (2.6)$$

It is this exponential dependence of the transmission coefficient  $T$  on the barrier width  $s$  that enables the atomic resolution images in the tunneling microscopy. It provides a sufficient signal, the tunneling current, for the atomic scale feedback control of the gap width  $s$  along the  $z$  direction.

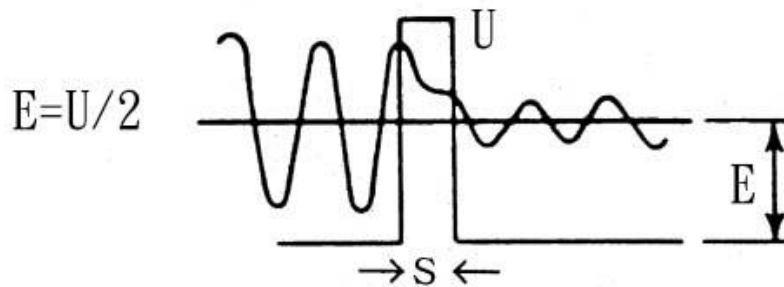


Fig. 2.4 Wave function  $\Psi(z)$  for an electron with kinetic energy  $E = U/2$  penetrating a potential barrier  $U$ .

## 2.3 Tip preparation

All STM tips are prepared with the traditional DC drop-off method, as shown in Fig. 2.4. The tips are typically made from cut-to-size tungsten (W) wire with diameters about 0.38 mm. The tungsten wire is electrochemically etched to produce the STM tips. It is an easy way to produce the tip. A piece of the tungsten wire and a cylindrical stainless steel are then inserted into a solution of 2M NaOH. The depth of the tungsten wire is about 1.5 ~ 2 mm below the solution level. A positive voltage about 7 V is applied to the tungsten wire. This wire acts as the anode while the cylindrical stainless steel acts as the cathode. This is shown in Fig. 2.5. At the anode and cathode the following reactions will take place:



The reaction etches the wire at the interface of air and the solution. This part then gets thinner and thinner, thereby forming a neck. The weight of the wire down below in the solution will eventually break the neck and causing the immersed portion of the tip to fall off. Therefore, a desired atomic tip is produced. Etching is usually stopped at this point by a feedback controller that senses the reduction in current. To remove the residual NaOH solution from the tip surface the tip are then been soaked in distilled water for 10 minutes and cleaned by pure methanol. The whole electrochemical etching process takes about 20 minutes.

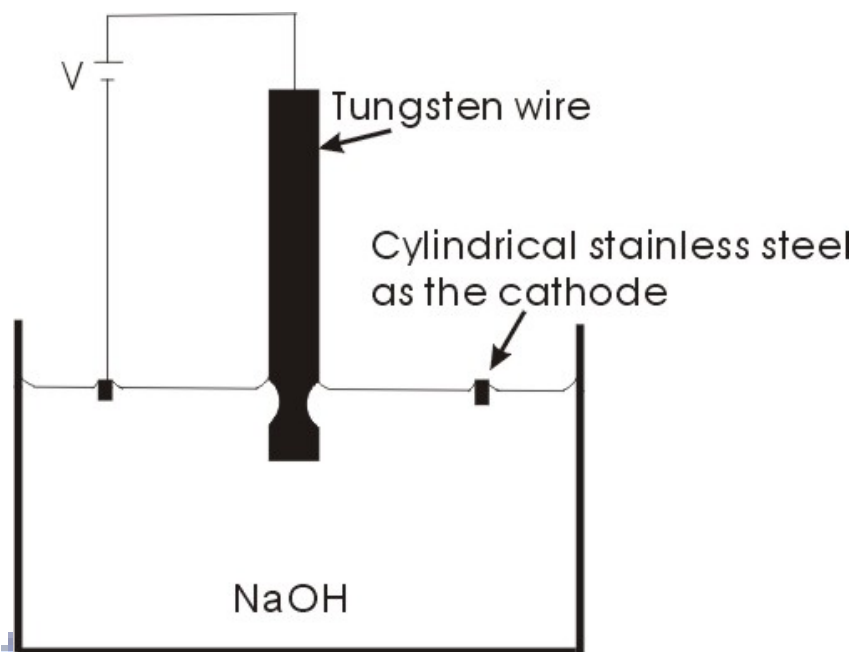


Fig. 2.5 The tungsten wire is electrochemically etched to produce atomic tips. A tungsten wire is vertically inserted in a solution of NaOH as the anode. A cylindrical stainless steel is also inserted in this solution as the cathode. A positive bias is placed on the tungsten wire. This etching takes about 20 minutes.



## 2.4 Sample preparation

Various sample treatments will be conducted depending upon the type of the sample that will be required for the experiment. The Si(100) samples used in our experiment were sliced from a antimony(Sb)-doped wafers with a dopant concentration of approximately  $1.5 \times 10^{15} \text{ cm}^{-3}$ . The misalignment of the wafer is about 0.1 degrees. Before loading the samples into the vacuum chamber, we blow off the dust on the surface of the samples with pure nitrogen gas so we don't have unwanted particles on the surface of the samples which could affect our measurements. After loading the samples to the UHV chamber, the samples are then being degassed for over 12 hours at  $\sim 900 \text{ K}$  using a small AC current (300 mA). After degassing, the sample was flashed at  $\sim 1450 \text{ K}$  for a few seconds in order to remove the oxide layer on the surface and form a dimerized clean Si(100)-(2x1) surface. After the direct heating, chlorine molecules were introduced through a leak valve and a stainless steel tube to the sample surface at room temperature to form the desired Cl-terminated Si(100)-(2x1) structure. A hot tungsten-spiral filament was used to produce atomic hydrogen. The filament was  $\sim 5 \text{ cm}$  away from the Si(100) substrate and heated to  $\sim 1800 \text{ K}$  when the chamber was backfilled for a period of time  $T$  with  $H_2$  to a pressure  $P$  of about  $2 \times 10^{-7} \text{ torr}$ . From the geometry of the filament and the samples, it was estimated that the incident angles of the H atoms was less than  $\sim 25^\circ$  from the normal. The apparent  $H_2$  exposure is presumably proportional to the actual dosage of hydrogen atoms on the surfaces.

## Chapter 3 Results and discussion

It was thought that H atoms adsorbed on the Si(100) surface with the substrate temperature been held at the room temperature during the H-atom exposure undergoes no diffusions [20]. But from our experiment, we have seen rare diffusions happening on the surface, an interaction that is assumed between the hydrogen atom and the chlorine atoms.

In the experiment, we exposed the Si(100) surface with  $\text{Cl}_2$  first, there was about 70 ~ 80% of the surface dangling bonds were Cl-terminated, as the time of exposing increases, the coverage of Cl increases. A significant amount of dark sites started to appear. These dark sites were thought to be single vacancies. From figure 3.1, it shows a systematic diagram starting with a Si atom missing from the dimer (assume it was Cl-terminated), as shown in (a), the chlorine molecule is attracted to this dimer and quickly breaks the sigma bond during the  $\text{Cl}_2$  exposure, (b). A  $\text{SiCl}_2$  is thus formed, as in (c). The  $\text{SiCl}_2$  desorbs and a single vacancy is then created, as in (d).

We have done two sets of experiments; one was on the pure Cl-terminated Si surface, the other was on the hydrogen exposed Cl-terminated Si surface. For the second set we exposed hydrogen atoms under  $1 \times 10^{-7}$  torr for about 2 minutes. In the next section, we shall discuss the dynamics of atom diffusions on the H-exposed surface at temperatures between 570K ~ 650K measured using ultra high vacuum-various temperature (UHV-VT) STM. We began by heating the Cl-saturated Si sample to the desired temperature and maintained it at this temperature during the whole data capturing. When the sample reached thermal equilibrium, we started focusing on a specific area and began scanning the sample. Throughout the capturing of the images we tried to keep the area being scanned in the same position. This was not an easy task as the image tends to drift away from the area and this will cost some time to adjust it back. In our experiments, it took about 80 seconds to scan one image. The whole process of obtaining one set of the data for various temperatures took about 30 minutes.

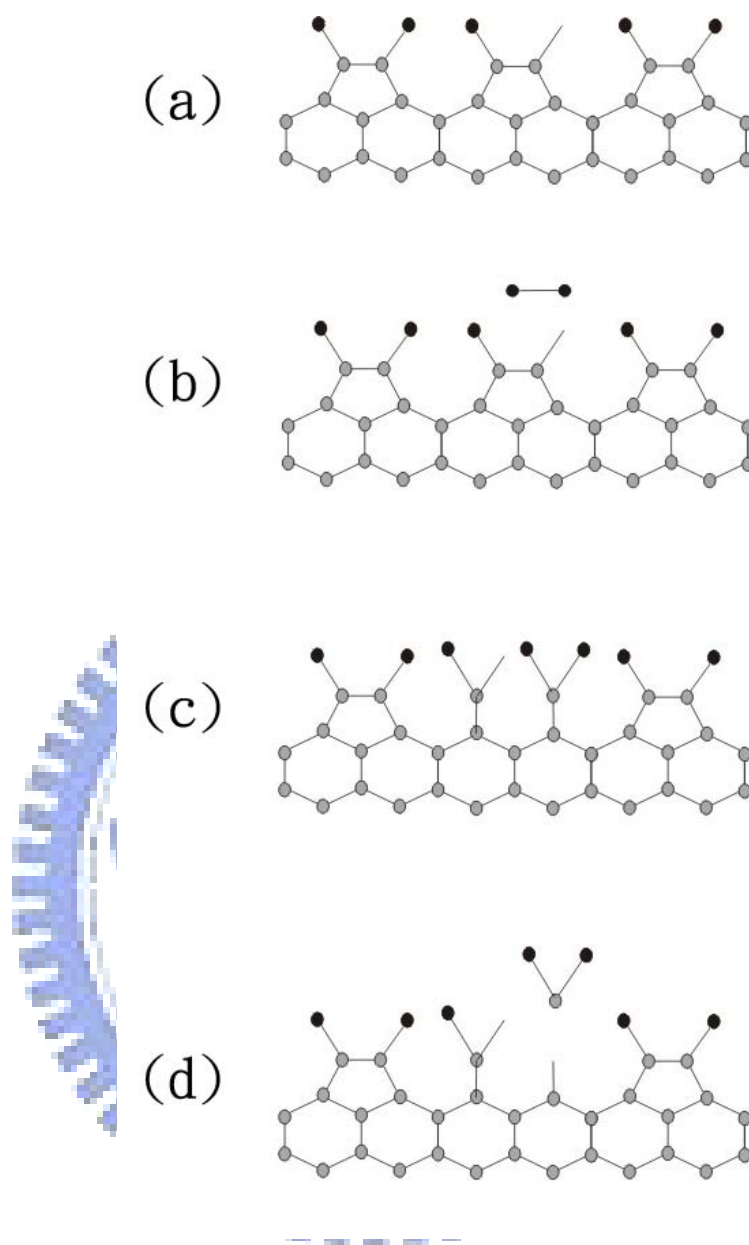


Fig.3.1 A systematic diagram showing the proposed formation of a single vacancy. (a) The initial configuration with one dangling bond of a dimer Cl-terminated. (b)-(c) A  $\text{Cl}_2$  breaks the sigma bond and adsorbs on the dangling bonds producing  $\text{SiCl}_2$ . (d) The  $\text{SiCl}_2$  desorbs and a single vacancy is created.

### 3.1 The dynamics of H-hopping

#### 3.1.1 Motion of H atoms at various temperatures

From our earlier report (as mentioned in section 1.5.4), we observed incident H-atom flux react with the Cl atoms that were adsorbed on the Si(100) surface, and the Cl adsorbents were extracted by the hydrogen gas atoms. In so, we believe that the single dark sites observed from the H-exposed images could have been hydrogen atoms, not vacancies. This was evident from the STM images obtained for both the H-exposed and non H-exposed sets, as the number of dark sites increased after we started exposing hydrogen atoms onto the Cl-terminated surface, as shown in figure 3.2. And so, in order to solve our query, we start by looking at the H-exposed sets. We shall discuss each temperature set separately.

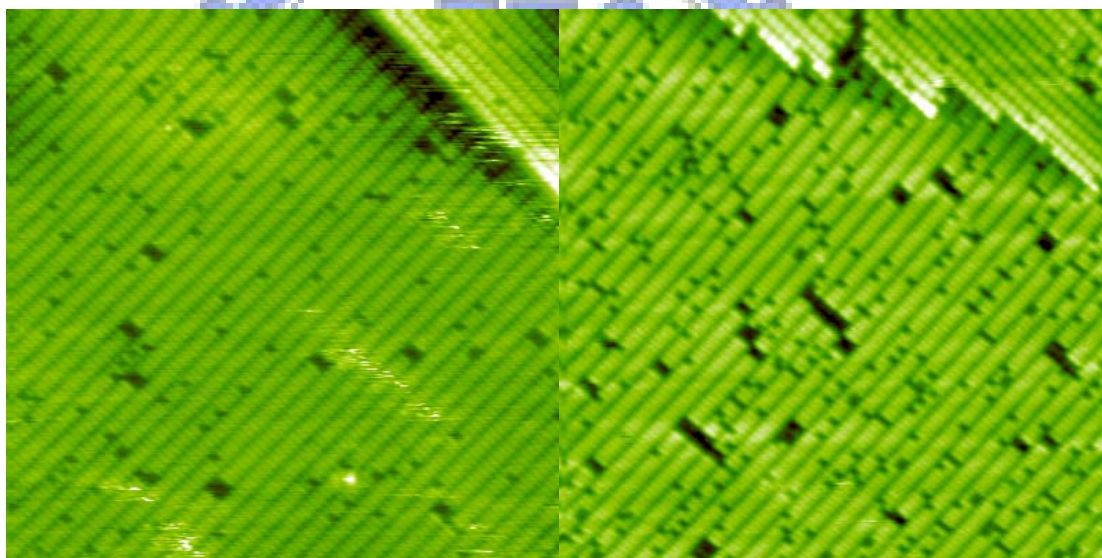


Fig.3.2 STM images of the non H-exposed (left) and the H-exposed (right) Si surface. It shows the difference in the number of dark sites on the surface. There was an increase in the number of dark sites found in the dimer rows after H-exposure. This image was taken at 570K with sample bias -2.2V.

#### (a) 570K

At this temperature, we took 21 images in a total of 30 minutes. Figure 3.3 shows one of the STM images we took at this temperature with a frame of an area under investigation. It shows the Si sample with dimer rows placed perpendicularly to each other on the steps. The dimers were made up of two chlorine atoms and were separated by a trough with the

adjacent dimer rows. There were single dark sites and defects in each and every one of the dimer rows. For the big defects, some even crosses over several dimer rows, and was fixed in position at all times. These large defects were empty spaces with silicon atoms missing from the first layer and leaves behind dangling bonds, causing the exposed chlorines to attach to the lower layer or adjacent silicon atoms rather than the first layer like other usual  $\text{SiCl}_2$ . We believe that these single dark sites are hydrogen atoms filling the space; therefore we shall in this section call these sites 'H-site'. These hydrogen sites were evenly spread throughout the image, and at this temperature, there were not much big defects either.

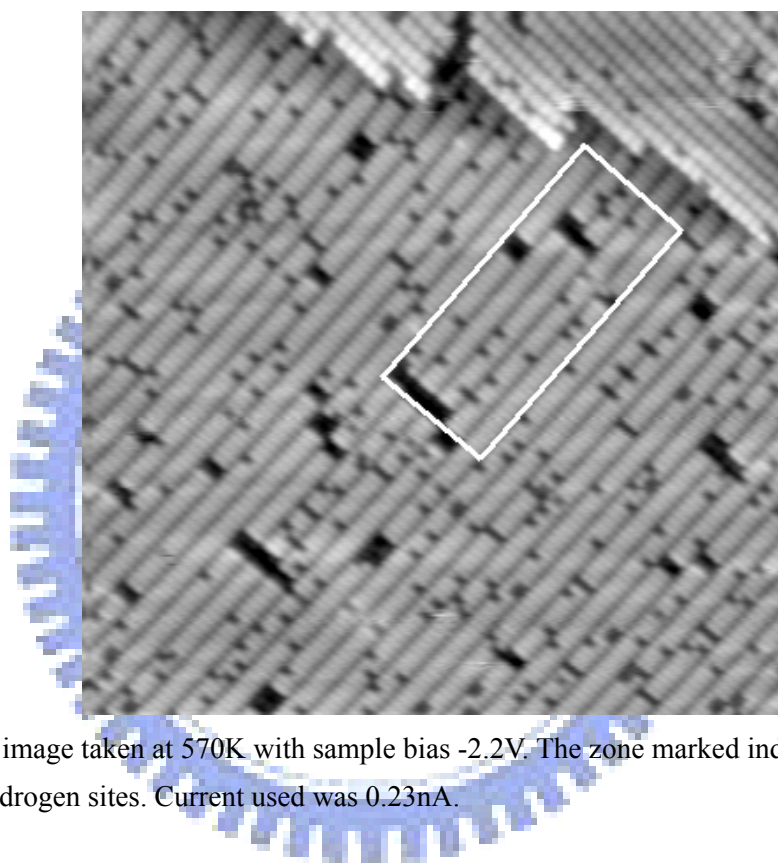


Fig.3.3 STM image taken at 570K with sample bias -2.2V. The zone marked indicates the area we traced our hydrogen sites. Current used was 0.23nA.

In this temperature, with defects remaining fixed at all times; it was clear that some of the H-sites started moving. Interestingly, it was not only one site movement, but several others have also been observed. There were three types of movement, namely *inter-dimer*, *intra-dimer*, and *inter-row*, see the sketch of figure 3.4. Figure 3.5 is a sequential STM image taken at this temperature demonstrating the movements of each dynamic. We shall give a short definition for the two basic hopping dynamics:

### 1. Intra-dimer

Intra-dimer hoppings is when a single atom jumps inside the same dimer. So there is only one direction it can jump to, either up or down, depends on the position that the single H-site is in.

### 2. Inter-dimer

Inter-dimer, also known as intra-row, means hopping along a dimer row. There are two directions it can jump to, left or right. Atoms are free to jump to any positions they want. There are no rules to their movement, or intentions to jump into more favorite positions. We shall discuss it in the later section where we discuss the statistics of the motions.

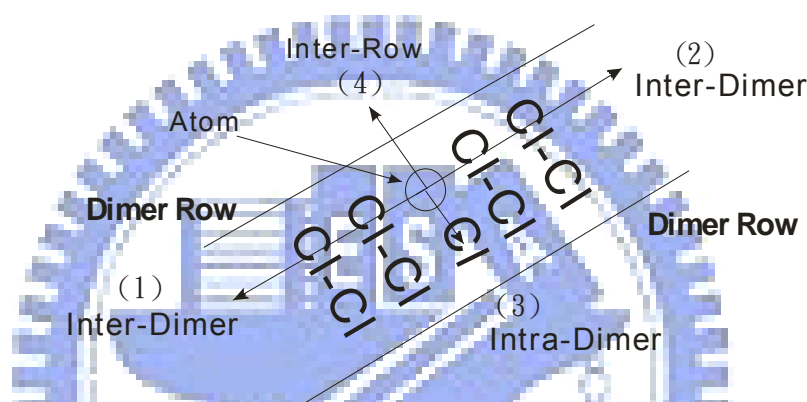


Fig.3.4 A simple sketch of the three types of dynamic motions in a dimer row. (1) and (2) are called inter-dimer hoppings when the atom moves in the direction parallel to (along) the dimer row, while motions perpendicular to the dimer row are called intra-dimer hoppings (3). (4) is the inter-row hopping as the atom jumps across to the adjacent dimer row.

From figure 3.5, we saw that initially there was no movement from the H-sites 1 and 2 in the first 90s, but site 3 and 4 both moved once from their original positions to the right. This movement is called the inter-dimer jump. After 180s, both sites 2 and 3 moved to the adjacent positions inside their respective dimers. These movements are called intra-dimer jumps. Site 1 jumped to the opposing dimer positions diagonally, this movement is said to have a long jump, or more precisely, a multiple jump. We believe this movement was a result of multiple single jumps in both dynamical directions in the short period of time. This will be recorded as a two step jump and one in each dynamics. 90 seconds later we saw site 1 moved again to the left. At this point all four H-sites have moved at least once. But from period 270s up to 450s none of the four sites moved again. In fact, most of them just moves once or twice and never moves again throughout the period of observation, which was very common at this low temperature. But while the four H-sites traced stop moving, it doesn't mean the other H-sites were fixed in their positions too, some of them still moved, and so

one site's motion doesn't affect the other. They were not related and were independent of their motions. A more detailed flow chart of the movements is shown in the appendix B.

Besides these two dynamics, there is a possibility for atoms to jump over the trough to the adjacent dimer rows, an event we call it *inter-row* hopping. Crossing over the dimer rows do sometimes occur, but very rare. Especially under low temperatures, this just never happens. It requires a large energy for the atoms to cross over to the adjacent dimer rows, and in low temperatures this energy is insufficient. So this will only happen at high temperature. As the temperature rises, not only the number of jumps will increase, the distance of the jumps will also increase, and as a result, the possibility of the multiple jumps happening will also rise. Inter-row jumps will also be very likely to happen because it now has enough energy to overcome the potential energy barrier.





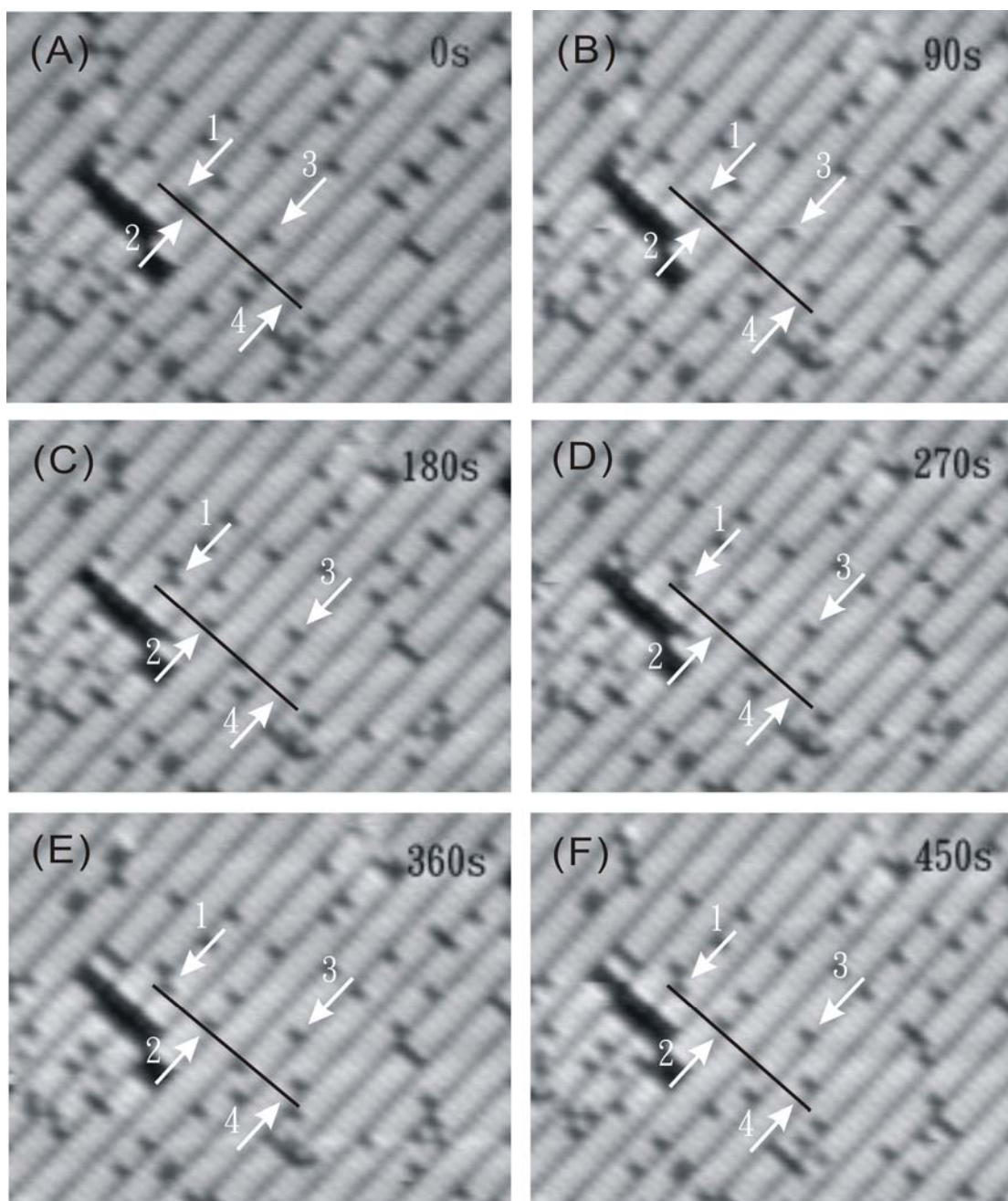


Fig.3.5 Six sequential STM images taken at 570K with sample bias -2.2V demonstrating the motions of single H-sites with time ranging from 0 second up to 450 seconds. Four of the H-sites were indicated with white arrows. These sites were given numbers from 1 to 4 for distinguishing them. From images (A)-(B), we saw sites 3 and 4 moved once to the right while sites 1 and 2 remain fixed in position. From image (C) we saw both sites 2 and 3 jumped to the adjacent positions in the same dimer respectively while sites 1 jumped diagonally to the opposing dimer in two steps. Site 4 remains fixed. At image (D) site 1 moved again to the left. From here onwards these four H-sites remain fixed in position as shown in images (E) and (F).



A total of 17 hydrogen sites were under the observation throughout the period. We tracked all 17 sites for their dynamic of motions. In the total of 17 sites traced, only 12 H-sites have moved in the inter-dimer directions, while only 10 H-sites have moved in the intra-dimer directions. In other words, not all the H-sites have moved at this temperature. In the period of 30 minutes, only 25 inter-dimer and 17 intra-dimer jumps were observed. We calculated the average hopping rate for both the inter-dimer and the intra-dimer dynamics separately. Because not all the H-sites were present throughout the period, therefore we have to calculate the hopping rate for every site first before we obtain the average hopping rate. To get the average rate, we sum up these single site movement rates and divide it by the number of sites found moving for each dynamic. Following is an example of our calculation:

**For H-site 1:**

Site 1 moved twice in the inter-dimer direction, once in the intra-dimer direction in the total period of 30 minutes and 11 seconds. Therefore we obtain the hopping rate as

*Inter-dimer:*

$$\frac{2}{(30 \times 60) + 11} = 1.1 \times 10^{-3} s^{-1}$$

*Intra-dimer:*

$$\frac{1}{(30 \times 60) + 11} = 5.5 \times 10^{-4} s^{-1}$$

**For H-site 2:**

Site 2 moved 3 times in the inter-dimer direction and 2 times in the intra-dimer direction. Therefore we obtain

*Inter-dimer:*

$$\frac{3}{(30 \times 60) + 11} = 1.7 \times 10^{-3} s^{-1}$$

*Intra-dimer:*

$$\frac{2}{(30 \times 60) + 11} = 1.1 \times 10^{-3} s^{-1}$$

We do these calculations for all 17 sites and sums up. Because not all the sites have moved at this temperature, therefore we only count the ones that have moved to get the average hopping rate, which worked out to be  $1.2 \times 10^{-3} s^{-1}$  for the inter-dimer hoppings, and  $9.4 \times 10^{-4} s^{-1}$  for the intra-dimer hoppings.

To obtain the needed activation energy and the attempt frequency prefactor for an atom to overcome the potential energy barrier, we shall use equation (1.7), the Arrhenius relation, as mentioned in section 1.4.1.1, which is

$$R = P \times e^{(-E_a/kT)},$$

where  $R$  is the hopping rate,  $P$  is the attempt frequency prefactor, and  $E_a$  is the activation energy.

To find the parameters we need to plot the graph of this relation. In doing so, we need to log the relation first, so we take log of the calculated average hopping rates and obtain -6.77 and -6.97 for the inter-dimer and intra-dimer hoppings respectively. So now we have For *Inter-dimer*:

$$-6.77 = \frac{-E_a}{8.617 \times 10^{-5} \times 570} + \ln P \dots \dots \dots (1)$$

For *Intra-dimer*:

$$-6.97 = \frac{-E_a}{8.617 \times 10^{-5} \times 570} + \ln P \dots \dots \dots (2)$$

We have now obtained the first point of our line for the plot. We shall work out the other points with the data obtained from other temperature sets.

#### (b) 600K

At this temperature, the density of H-sites is about the same. But evidently the change of events increases. More and more H-sites were found moving. Noticeably the number of jumps has slightly increased. Either in inter-dimer jumps or in intra-dimer jumps. In both situations, almost every single one of the traced H-sites moved at least twice within the period, also two multiple step jumps in the inter-dimer directions were firstly observed. We also had our first inter-row jump.

Under this temperature, we picked 20 H-sites and found only 18 sites moved in the inter-dimer direction, while 17 were observed in the intra-dimer direction in a period of 28 minutes and 27 seconds. Again we show an example of the calculations for the single H-site hopping rate for this temperature:

**For H-site 1:**

Site 1 moved five times in the inter-dimer direction, twice in the intra-dimer direction in the total period of 28 minutes and 27 seconds. Therefore we obtain the hopping rates as

*Inter-dimer:*

$$\frac{5}{(28 \times 60) + 27} = 2.9 \times 10^{-3} s^{-1}$$

*Intra-dimer:*

$$\frac{2}{(28 \times 60) + 27} = 1.2 \times 10^{-3} s^{-1}$$

**For H-site 2:**

Site 2 moved 3 times in the inter-dimer direction and 3 times in the intra-dimer direction. Therefore we obtain

*Inter-dimer:*

$$\frac{3}{(28 \times 60) + 27} = 1.8 \times 10^{-3} s^{-1}$$

*Intra-dimer:*

$$\frac{3}{(28 \times 60) + 27} = 1.8 \times 10^{-3} s^{-1}$$

As usual, we do these calculations for all the 20 H-sites and sums up. Same as the previous set, not all the H-sites moved. So to get the average hopping rate, we need to divide the summation with the 18 and the 17 H-sites found moving in the inter-dimer and intra-dimer directions respectively. It worked out to be  $2.2 \times 10^{-3} s^{-1}$  for the inter-dimer hoppings, and  $1.2 \times 10^{-3} s^{-1}$  for the intra-dimer hoppings. Take the log of both we get -6.13 and -6.69 respectively. So now we have obtained our second point for the plot, as

*For Inter-dimer:*

$$-6.13 = \frac{-E_a}{8.617 \times 10^{-5} \times 600} + \ln P \dots\dots\dots (3)$$

*For Intra-dimer:*

$$-6.69 = \frac{-E_a}{8.617 \times 10^{-5} \times 600} + \ln P \dots\dots\dots (4)$$

### (c) 615K

At this relative high temperature, H-sites were really started to get moving. As the temperature increase, you can see these H-sites jumping at a much faster pace. There were hopping events happening in almost every place of the image. We found surprisingly there were some H-sites jumps in and/or out of the frame, or more correctly, disappears. By the next time you trace it, it was gone, disappeared from their previous positions. H-sites don't go disappearing for any reasons. Due to the higher energy source, it is very likely that some of the H-sites will jump out of the frame from where you have been tracking them. Some of them will be found down a few dimers, some of them might have jumped to the adjacent rows. It is also equally likely for H-sites to jump into the frame of examining. Sometimes you will find there were dark sites suddenly appearing in the area where you traced your H-sites. These sudden appeared sites were moved in from other areas due to the higher rate of movement. It is possible that these sites were flowing around on the surface before they insert themselves into the first layer. This situation was very common at high temperatures.

Under this temperature we traced 30 H-sites for our observations in a period of 28 minutes and 19 seconds. Figure 3.6 are some STM images arranged sequentially showing some of the hopping events happened during the time of our observations. We can see very clearly throughout the period, H-sites moved from the initial image (a) to the final image (h). We found all 30 sites moved in the inter-dimer direction, but only 27 found moved in the intra-dimer direction. One inter-row jump was again observed at this temperature.

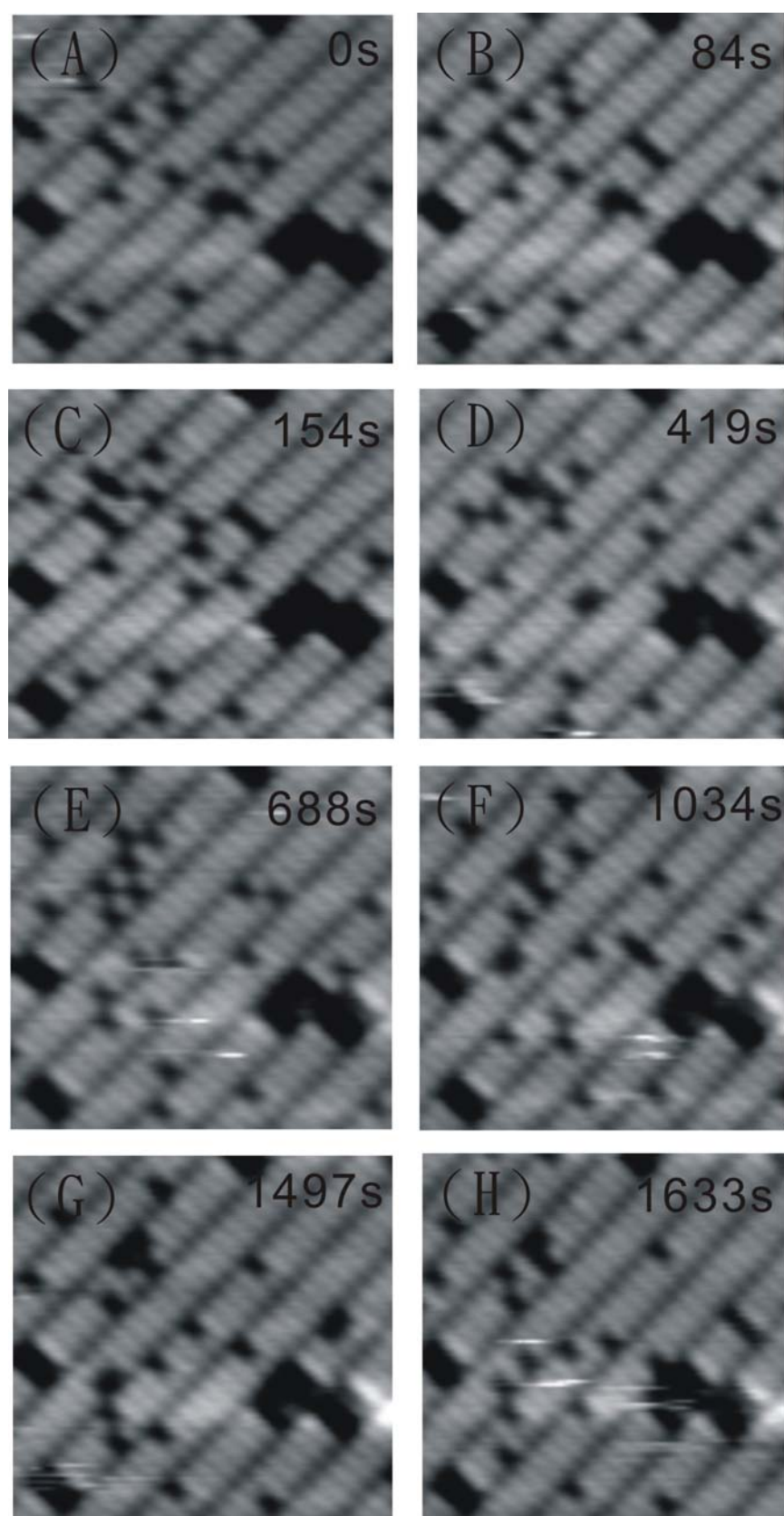


Fig.3.6 Eight sequential images taken at 615K with sample bias -2.2V. From (A) to (H) it shows the motions of H-sites throughout the time on the Cl-saturated Si(100)-(2x1) surface. It gives a good indication on the H-site movements. The current used was 0.23nA.

And so for the calculations:

**For H-site 1:**

Site 1 moved 5 times in the inter-dimer direction, 3 times in the intra-dimer direction in the total period of 28 minutes and 19 seconds. Therefore we obtain the hopping rate as for the

*Inter-dimer:*

$$\frac{5}{(28 \times 60) + 19} = 2.9 \times 10^{-3} s^{-1}$$

*Intra-dimer:*

$$\frac{3}{(28 \times 60) + 19} = 1.8 \times 10^{-3} s^{-1}$$

**For H-site 2:**

Site 2 moved 6 times in the inter-dimer direction and 3 times in the intra-dimer direction. Therefore we obtain

*Inter-dimer:*

$$\frac{6}{(28 \times 60) + 19} = 3.5 \times 10^{-3} s^{-1}$$

*Intra-dimer:*

$$\frac{3}{(28 \times 60) + 19} = 1.8 \times 10^{-3} s^{-1}$$

For the average hopping rate, we divided the summation and it worked out to be  $3.5 \times 10^{-3} s^{-1}$  for the inter-dimer hoppings, and  $1.8 \times 10^{-3} s^{-1}$  for the intra-dimer hoppings. Take the log of both we obtain -5.67 and -6.34 respectively. So now we have obtained our third point of the plot, as

For *Inter-dimer*:

$$-5.67 = \frac{-E_a}{8.617 \times 10^{-5} \times 615} + \ln P \dots\dots\dots (5)$$

For *Intra-dimer*:

$$-6.34 = \frac{-E_a}{8.617 \times 10^{-5} \times 615} + \ln P \dots\dots\dots (6)$$

(d) 630K

At this temperature the H-sites moved almost in every single one of the images observed. The frequency of the jumps were increased, more sites were jumping in and out of the frame. A few was out of the sight, and a few was newly joined. But majority of the H-sites stayed within the frame, so it was not much a problem tracking them. Under this temperature H-sites started to get involved more in the long distance jumps. In other words, more multiple step jumps were observed, some have been observed jumping as far as six dimers in the inter-dimer direction. Detail of this will be discussed later. As usual we obtain the average hopping rate for this temperature by first finding the hopping rates of H-sites traced. We picked a total of 18 H-sites and traced them in a period of 27 minutes and 19 seconds. This time, all the sites have moved in both dynamics. So for the calculations:

**For H-site 1:**

Site 1 moved 18 times in the inter-dimer direction, 8 times in the intra-dimer direction in the total period of 27 minutes and 19 seconds. Therefore we obtain the hopping rate as for the

*Inter-dimer:*

$$\frac{18}{(27 \times 60) + 19} = 1.1 \times 10^{-2} s^{-1}$$

*Intra-dimer:*

$$\frac{8}{(27 \times 60) + 19} = 4.9 \times 10^{-3} s^{-1}$$

**For H-site 2:**

Site 2 moved 21 times in the inter-dimer direction and 10 times in the intra-dimer direction. Therefore we obtain

*Inter-dimer:*

$$\frac{21}{(27 \times 60) + 19} = 1.3 \times 10^{-2} s^{-1}$$

*Intra-dimer:*

$$\frac{10}{(27 \times 60) + 19} = 6.1 \times 10^{-3} s^{-1}$$

For the average hopping rate, after dividing the summations it worked out to be  $9.4 \times 10^{-3} s^{-1}$  for the inter-dimer hoppings, and  $3.4 \times 10^{-3} s^{-1}$  for the intra-dimer hoppings. Take the log of both we obtain -4.67 and -5.70 respectively. So now we have obtained our forth point for the plot, as

For *Inter-dimer*:

$$-4.67 = \frac{-E_a}{8.617 \times 10^{-5} \times 630} + \ln P \dots\dots\dots (7)$$

For *Intra-dimer*:

$$-5.70 = \frac{-E_a}{8.617 \times 10^{-5} \times 630} + \ln P \dots\dots\dots (8)$$

### (e) 650K

For this temperature, H-sites were moving in a very fast pace. Some defects were observed to appear only after a while as the chlorines seen to be extracted. All tracked H-sites moved at least once in every single one of the images observed. The rate is so high that it was difficult to trace them. A lot of them have disappeared through the period of observation; some of them appeared out of no where. With such a high jumping rate, the jumping distances were much longer, seven as been observed, and the frequency of the multiple jumps observed were more often. Although it was not easy to track them, we still managed to pick out some H-sites that allowed us to observe throughout the period.

We managed to pick out a total of 18 H-sites under this temperature in a period of 23 minutes and 56 seconds. Again, all the sites have moved in both dynamics. For the calculations:

#### For H-site 1:

Site 1 moved 40 times in the inter-dimer direction, 9 times in the intra-dimer direction in the total period of 23 minutes and 56 seconds. Therefore we obtain the hopping rate as for the

*Inter-dimer*:

$$\frac{40}{(23 \times 60) + 56} = 2.8 \times 10^{-2} s^{-1}$$

*Intra-dimer*:

$$\frac{9}{(23 \times 60) + 56} = 6.3 \times 10^{-3} s^{-1}$$



**For H-site 2:**

Site 2 moved 39 times in the inter-dimer direction and 9 times in the intra-dimer direction. Therefore we obtain

*Inter-dimer:*

$$\frac{39}{(23 \times 60) + 56} = 2.7 \times 10^{-2} s^{-1}$$

*Intra-dimer:*

$$\frac{9}{(23 \times 60) + 56} = 6.3 \times 10^{-3} s^{-1}$$

As usual, for the average hopping rate, after dividing the summations it worked out to be  $2.52 \times 10^{-2} s^{-1}$  for the inter-dimer hoppings, and  $5.1 \times 10^{-3} s^{-1}$  for the intra-dimer hoppings. Take the log of both we obtain -3.68 and -5.27 respectively. So now we have obtained our fifth and final point for the plot, as

For *Inter-dimer*:

$$-3.68 = \frac{-E_a}{8.617 \times 10^{-5} \times 650} + \ln P \dots\dots\dots (9)$$

For *Intra-dimer*:

$$-5.27 = \frac{-E_a}{8.617 \times 10^{-5} \times 650} + \ln P \dots\dots\dots (10)$$

### 3.1.2 Arrhenius plot and activation energy for the H-exposed set

With all the necessary points obtained, we are now ready to plot the line and find out the activation energy as well as the prefactor for the set with H-exposure. We shall plot both the inter-dimer and the intra-dimer dynamics separately to get separate activation energy values.

From temperature 570K up to 650K, with all the average hopping rates obtained, we make an Arrhenius plot with the log of the average hopping rates as opposed to the inverse of the temperatures. Both lines have been plotted on the same graph:

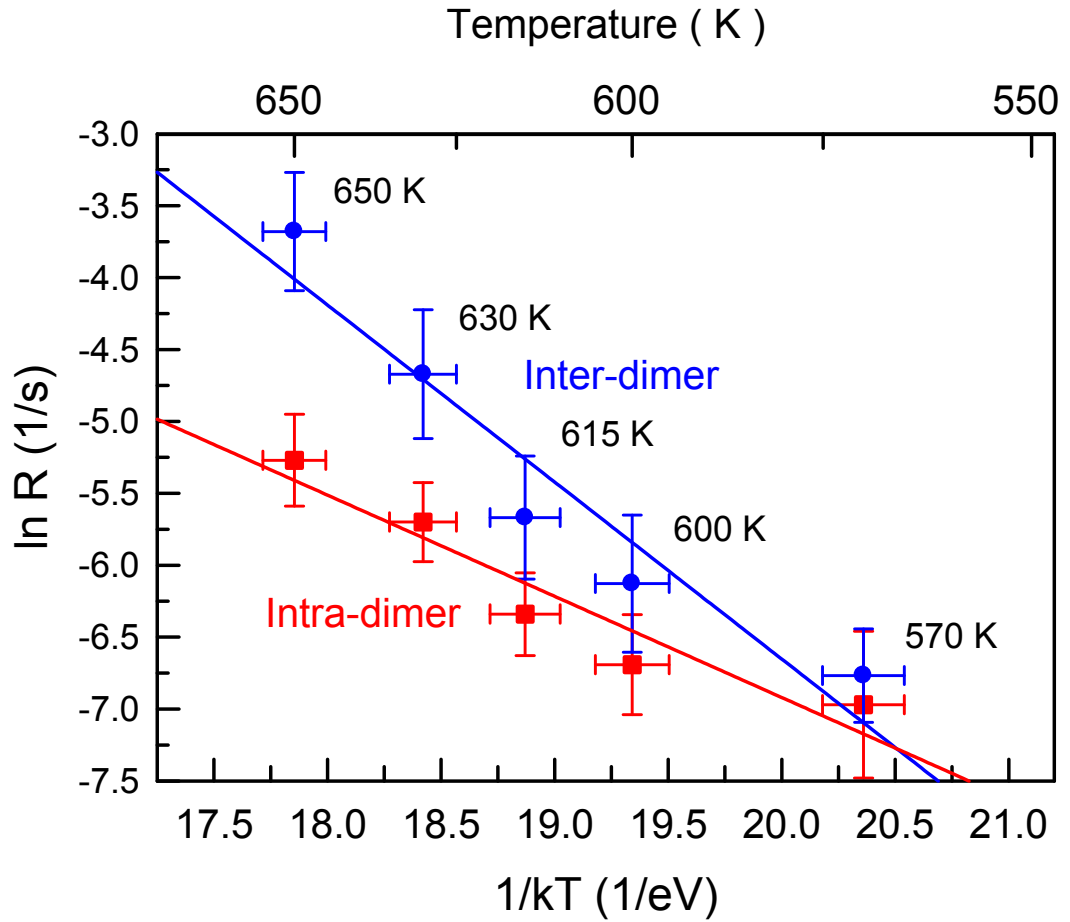
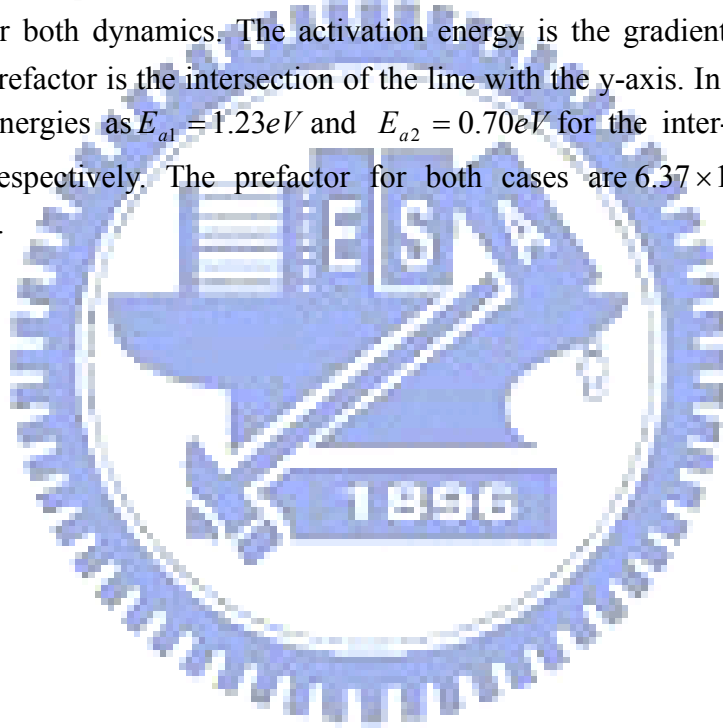


Fig.3.7 Arrhenius plot for the H-exposed hopping rates of H-sites. Top line is the inter-dimer hoppings and bottom line is the intra-dimer hoppings. Corresponding temperatures are stated next to the points. Top x-axis is the temperature while bottom x-axis is the inverse temperature. Y-axis is the logged hopping rate. The activation energy is the gradient of the line, and the frequency prefactor is the y-axis intercept of the line. We obtained the activation energies as  $1.23eV$  and  $0.70eV$ , and the frequency prefactor as  $6.37 \times 10^7 s^{-1}$  and  $1.28 \times 10^3 s^{-1}$  for the two dynamics respectively.

From figure 3.7, we see all the points lay more or less close to the line with the reasonable range of errors. For the calculation of the vertical error bars we took the difference between the H-sites with the biggest (or smallest) hopping rate calculated and the average hopping rate values at each temperature. And for the horizontal error bars we estimated it to be  $\pm 5K$  for all the points. In a well defined straight line fashion it shows a corresponding relation between the temperature and the hopping rates. It clearly shows, as the temperature rise, the rate of movement increases too. It also shows that the proportion of the rate of increase is very similar for both cases. Almost a constant increasing rate appears especially at the higher temperatures.

From the equation of the lines we can determine the activation energy and the prefactor for both dynamics. The activation energy is the gradient of the line, while the frequency prefactor is the intersection of the line with the y-axis. In this case we obtain the activation energies as  $E_{a1} = 1.23eV$  and  $E_{a2} = 0.70eV$  for the inter-dimer and intra-dimer dynamics respectively. The prefactor for both cases are  $6.37 \times 10^7 s^{-1}$  and  $1.28 \times 10^3 s^{-1}$  respectively.



## 3.2 Statistics of H-exposed hoppings

It is interesting to see how H atoms behave on the Si(100) Cl-terminated surface. One way of finding out how they behave is by making a plot like we did in the previous sections. Another way of doing it is by collecting the data from each set and makes them into a chart for easier comparisons. Either way will give an insight into the behavior of the H atoms.

We have collected some information regarding the motions and the movements of H-sites from each temperature sets. In this section we shall examine the data gathered. This will provide us a few more ideas in the dynamics of H-hopping.

### 3.2.1 Raw data

We have counted a total of 1562 observations for the H-site movements from 570K up to 650K. A table of summary is shown in the next page.

From the summary made, we can see clearly there was an increase in the total number of hopping events happened in both the inter-dimer direction and the intra-dimer directions through the rise in temperature. Also an interesting observation was the number of inter-row jumps took place. When at low temperature 570K where only a few jumps made, the chance for an inter-row jump to happen was very small. From the period we observed, we didn't see any of it took place. At low temperatures there was not enough energy for the H-site to overcome the energy barrier and jump cross dimer rows. But when we got to 600K, we started to see it was more possible for the event to happen. From this temperature onwards there was at least one inter-row hopping in every temperature set. H-sites were then having enough energy to conquer the energy barrier and jump cross the rows. And as we got higher in temperature, the possibility for the cross to happen gets higher too. At temperature 650K we saw two inter-row hoppings happened. This might seen as a small amount, but it was twice the jumps made in the previous temperatures, and also in a slight shorter time. We believe, had the time of observation been longer, much more of the inter-row jumps will take place.

H-hopping (with H-exposure)						$R=n1/(qxt)$	$R=n2/(qxt)$
	No. of H-sites traced ( $q$ ) (inter/intra/total)	Period (s) ( $t$ )	Inter-dimer observed ( $n1$ )	Intra-dimer observed ( $n2$ )	Inter-row observed	Hopping rates Inter-dimer ( $R$ ) (1/s)	Hopping rates Intra-dimer ( $R$ ) (1/s)
570K	12/10/17	1811	25	17	0	$1.15 \times 10^{-3}$	$9.40 \times 10^{-4}$
600K	18/17/20	1707	67	36	1	$2.18 \times 10^{-3}$	$1.24 \times 10^{-3}$
615K	30/27/30	1699	176	81	1	$3.45 \times 10^{-3}$	$1.76 \times 10^{-3}$
630K	18/18/18	1639	276	99	1	$9.36 \times 10^{-3}$	$3.35 \times 10^{-3}$
650K	18/18/18	1436	652	133	2	$2.52 \times 10^{-2}$	$5.14 \times 10^{-3}$

Table 3.1 A summary of the H-exposed Si(100) Cl-terminated surface hopping data obtained from the various temperature sets.

### 3.2.2 Preference of hopping movements

We are interested in the case of inter-dimer hoppings in which if the H-sites prefer to move in any one of the directions. There are only two directions that a H-site can jump to, either to the left or right, which is simply the code name for hopping into or out of the steps, depending on the situation. From the statistics we obtained shows an increase in jumping distances as the temperature rises. Figure 3.8 to 3.12 are the hopping directions and the various jumping distances observed plotted on the same graph for each temperature sets. Clearly as in temperature 570K only single jumps existed. At 600K two double jumps observed in each direction, but the majority of the jumps are still single jumps. When temperature rises to 615K, more and more of the multiple step jumps appeared. Still the majority of the jumps are single jumps. The longest jumping distance at this point is triple jumps which appeared twice. When we get to 630K, the hopping distances are getting longer and longer. Even though there is still quite a few amount of single jumps committed, a significant amount of multiple jumps are also observed. There is only about 60% of the H-site jumps are still single jump, the rest are multiple jumps in various distances. This is a big decrease compared to an average of 90% single jumps committed from previous temperatures. At temperature 650K, this majority of single lattice spacing H-site jumps no longer holds, multiple jumps have since greatly increased. With an average percentage of 65% the majority of H-site jumps are now dominated by multiple jumps. Jumps as far as 7 lattice spacings are observed. The sites are now hopping in a very high rate.

Figure 3.13 shows that with the total number of 685 inter-dimer hopping events observed in all temperatures, the percentages of both left and right direction of hoppings appeared. As you can see, the percentage is very even, with 49.2% for the left, 50.8% for the right directions. This again coincides with data obtained from an earlier experiment, in which 49.5% and 50.5% were obtained for both directions respectively at high temperatures (see appendix for details of the results).

So from these results we can now conclude that the distances of single H-site jumps are temperature dependent, and the direction of jumps are equivalent in both directions.

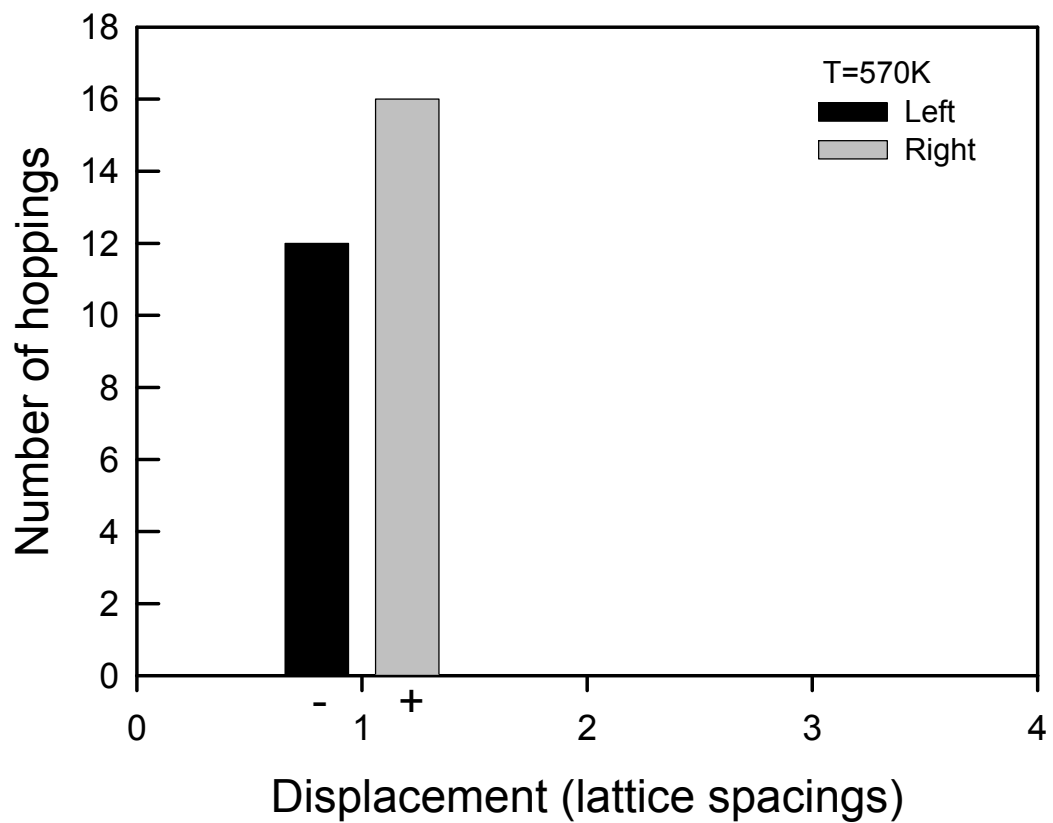


Fig.3.8 Number of inter-dimer hoppings observed at 570K against the jumping distances. Dark bar and the minus sign symbolizes left direction and the grey bar with the plus sign symbolizes right direction (direction respects to the images). Clearly only single jumps were observed at this temperature for both directions. No multiple jumps were found.

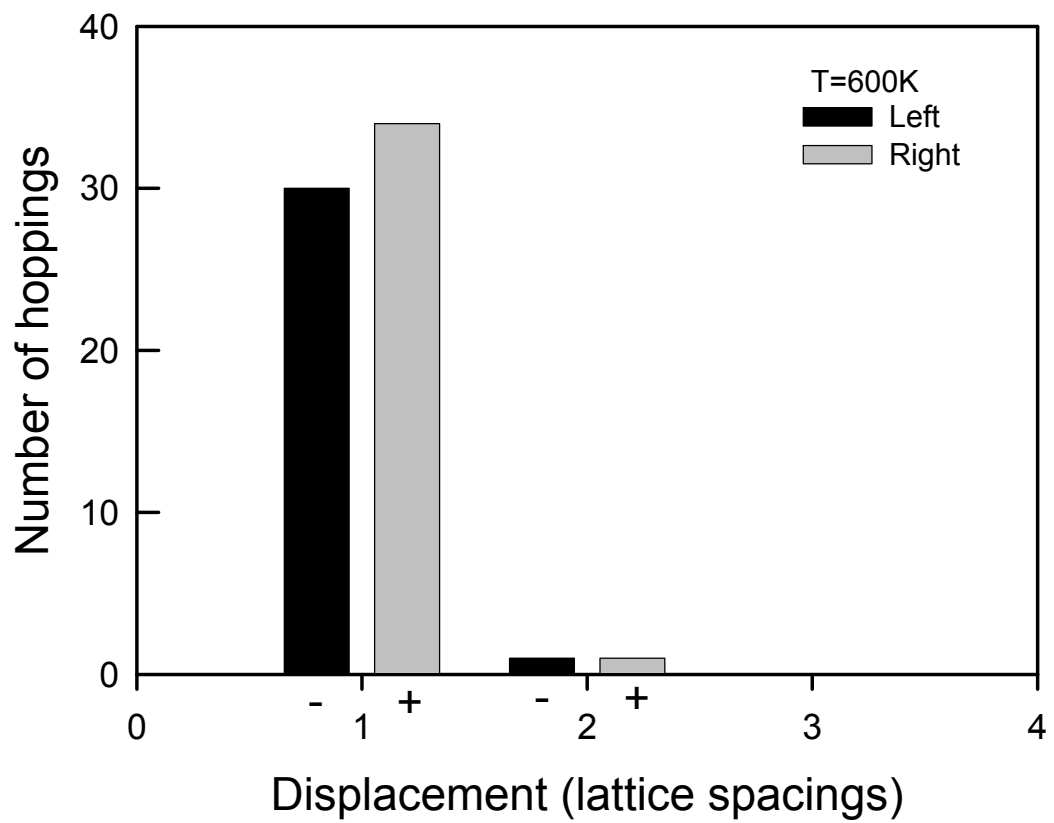


Fig.3.9 Number of inter-dimer hoppings observed at 600K. This time we saw two double jumps took place in each directions. The number of jumps increased as a result of rise in temperature.



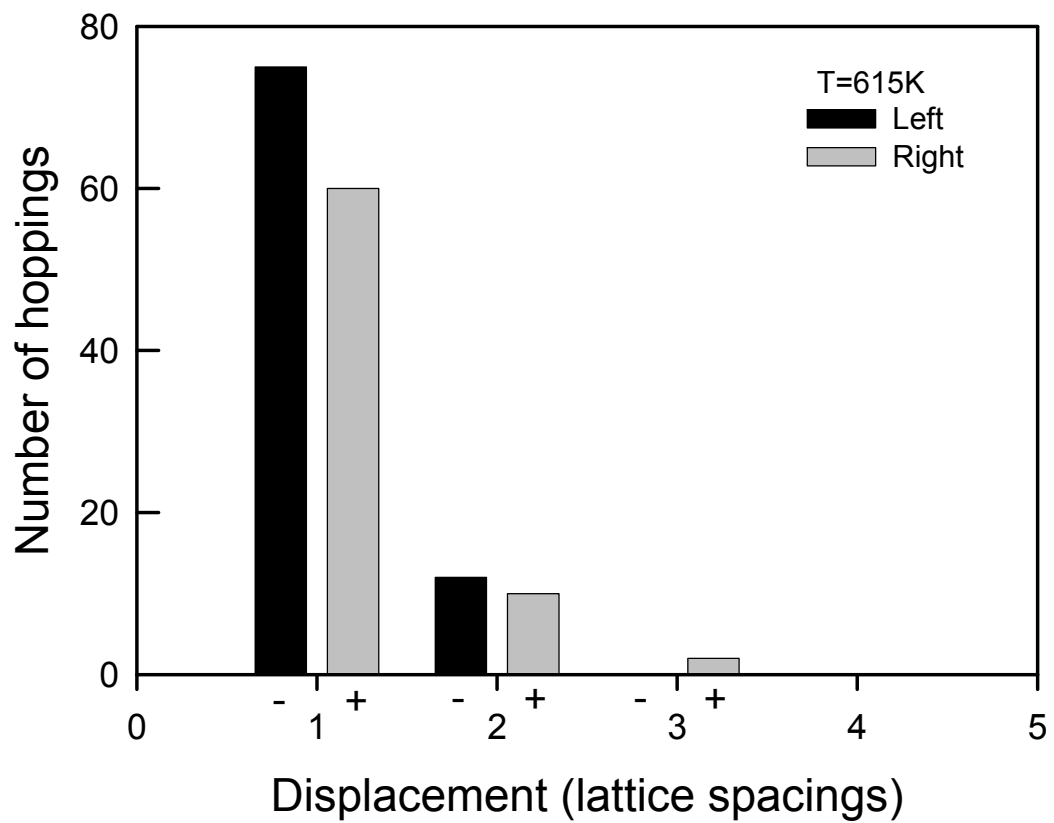


Fig.3.10 Number of inter-dimer hoppings observed at 615K. At this temperature we saw triple jump happened once in the right directions. The number of single and double jumps increased as well.

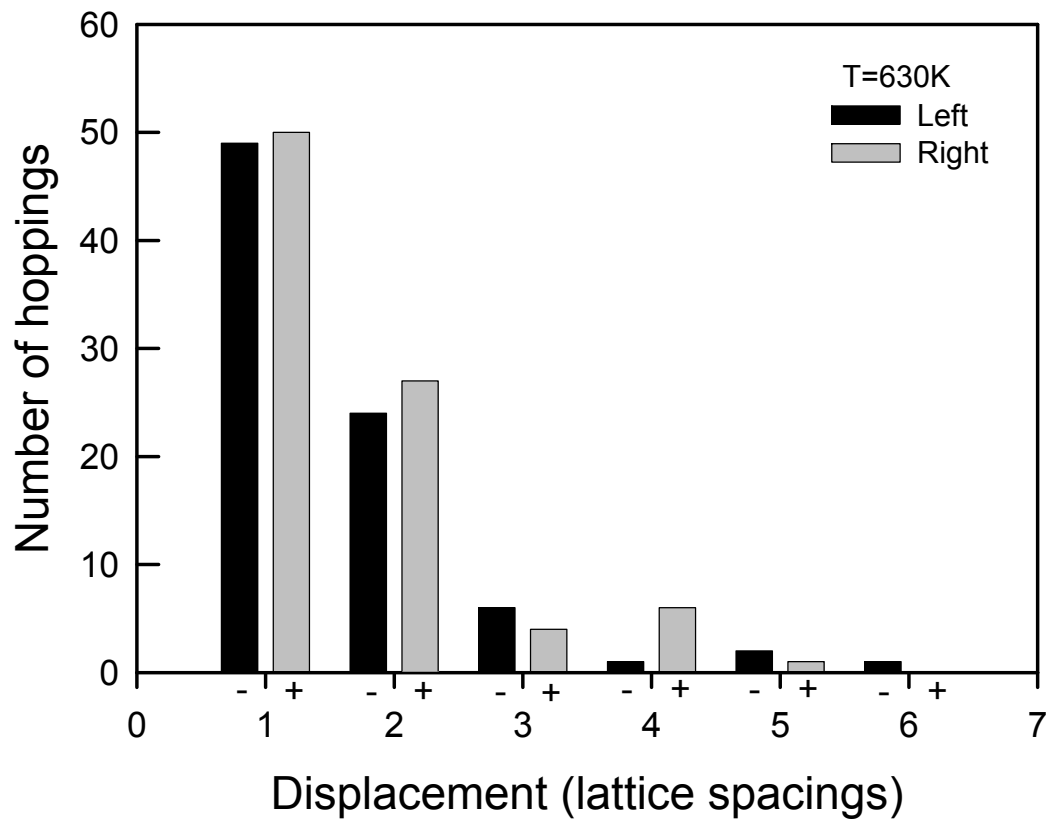


Fig.3.11 Number of inter-dimer hoppings observed at 630K. The number and distances of multiple jumps have increased dramatically since the last temperature. We saw a multiple jump as far as 6 dimers. Jumps in other distances have also increased, but the number of single jumps observed has decreased.

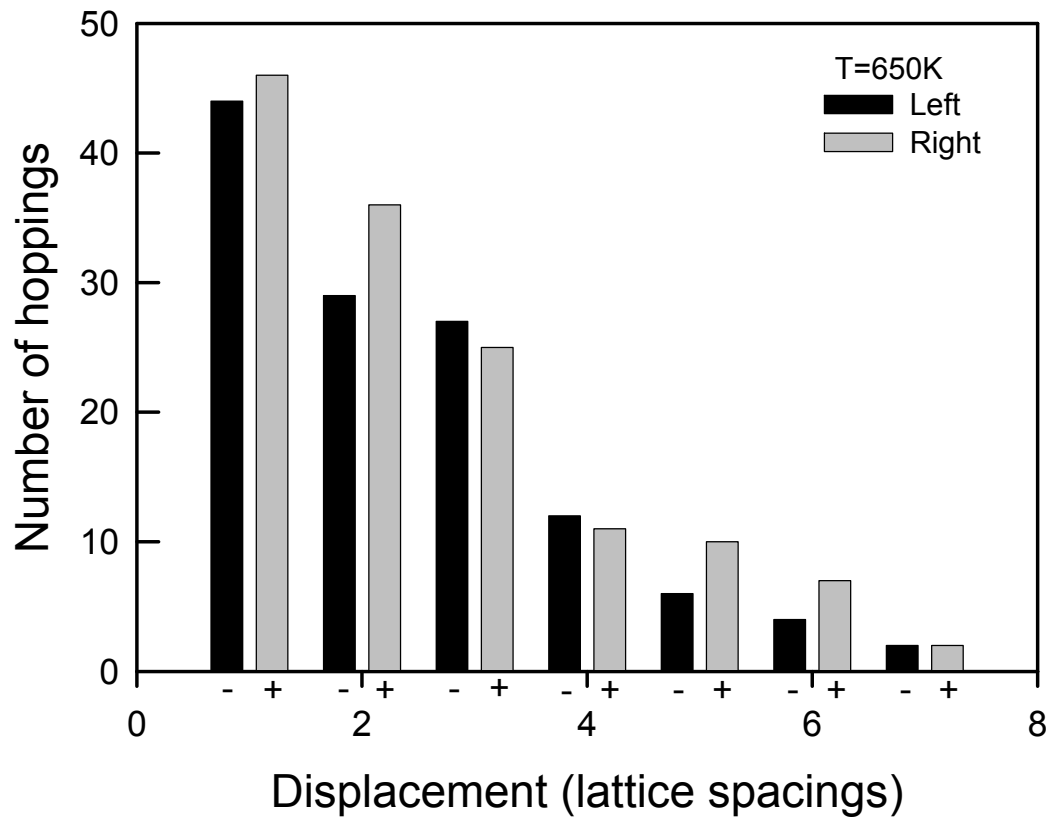


Fig.3.12 Number of inter-dimer hoppings observed at 650K. At this temperature it was dominated by multiple jumps, with a majority of 65% were multiple step jumps. Single step jumps have decreased from around 75% to 35% since previous temperatures. The maximum jumping distance observed was 7 dimer spacings which happened four times.

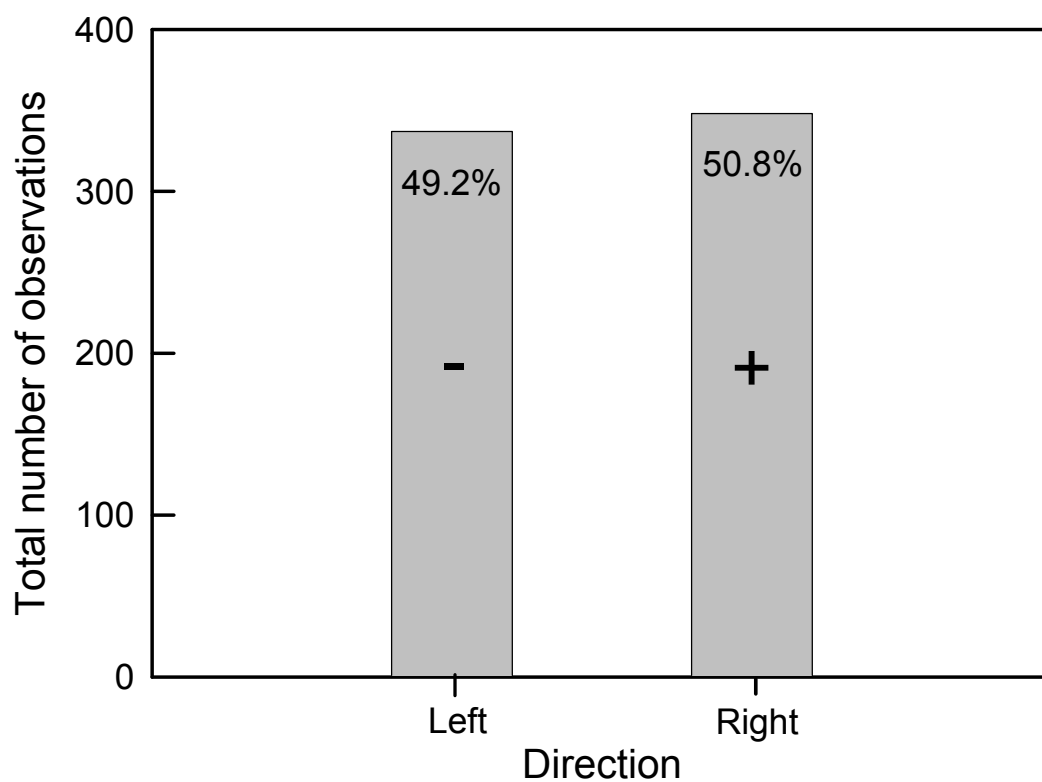


Fig.3.13 Total number of inter-dimer hoppings observed with all temperatures in both directions. The percentages of hopping in each direction are shown. Minus sign represents the left direction jumps while plus sign represents the right direction jumps. According to the result, it showed there were no preferences for the H-sites to jump in either direction.

### 3.3 Results on non H-exposed hoppings

In this section we will find out if our assumptions in the beginning about these “single vacancies” we have thought they were on the Si(100)-2x1 Cl-terminated surface are actually hydrogen atoms. To verify our assumptions we needed to do an experiment on pure Si(100) Cl-terminated surface without the exposure of hydrogen atoms. This way we will have a very good idea on how the dark sites behave on the clean Si(100) Cl-terminated surface knowing the single dark sites we have seen moving on the surface is actually an atom and not vacancy.

We took data at temperatures from 570K up to 630K. This will help us in comparing the data with the previous set where we have exposed hydrogen atoms on the Si(100) Cl-terminated surface. This experiment, like the previous, was also done with the UHV-VT STM. We add currents to the sample and heat it to a certain temperature before we start our observations. All experiments were done in the same way with the increase in temperature. Following table 3.2 is a summary of the data obtained with the hopping rates for both dynamics calculated.

This time we traced 9~12 single dark sites in a time of 21~24 minutes. We traced their movement in both inter-dimer directions as well as the intra-dimer directions. The hopping rates we calculated were slightly lower than the previous set at about half an inverse second. But overall the results corresponded to the previous results. As expected, hopping rates increases as temperature rises. No surprises were found. Again, we make a plot with the log of the hopping rates against the inverse of the temperatures using the Arrhenius relations. The resulting graph is given in figure 3.14. From the plot we find that the activation energies and the frequency prefactors as  $E = 1.14\text{eV}$  and  $2.83 \times 10^7 \text{ s}^{-1}$  for the inter-dimer hoppings, while for the intra-dimer hoppings  $E = 0.62\text{eV}$  with  $4.83 \times 10^2 \text{ s}^{-1}$ .

H-hopping (without H-exposure)					$R=n1/(qxt)$	$R=n2/(qxt)$
	No. of H-sites traced ( $q$ ) (inter/intra/total)	Period (s) ( $t$ )	Inter-dimer observed ( $n1$ )	Intra-dimer observed ( $n2$ )	Hopping rates Inter-dimer ( $R$ ) (1/s)	Hopping rates Intra-dimer ( $R$ ) (1/s)
570K	8/7/9	1461	31	19	$2.65 \times 10^{-3}$	$1.67 \times 10^{-3}$
600K	9/9/9	1352	88	45	$7.23 \times 10^{-3}$	$3.70 \times 10^{-3}$
615K	11/10/11	1312	114	48	$1.00 \times 10^{-2}$	$4.29 \times 10^{-3}$
630K	11/11/11	1457	450	89	$2.80 \times 10^{-2}$	$5.55 \times 10^{-3}$

Table 3.2 A summary of the non H-exposed Si(100) Cl-terminated surface hopping data obtained from various temperature sets.

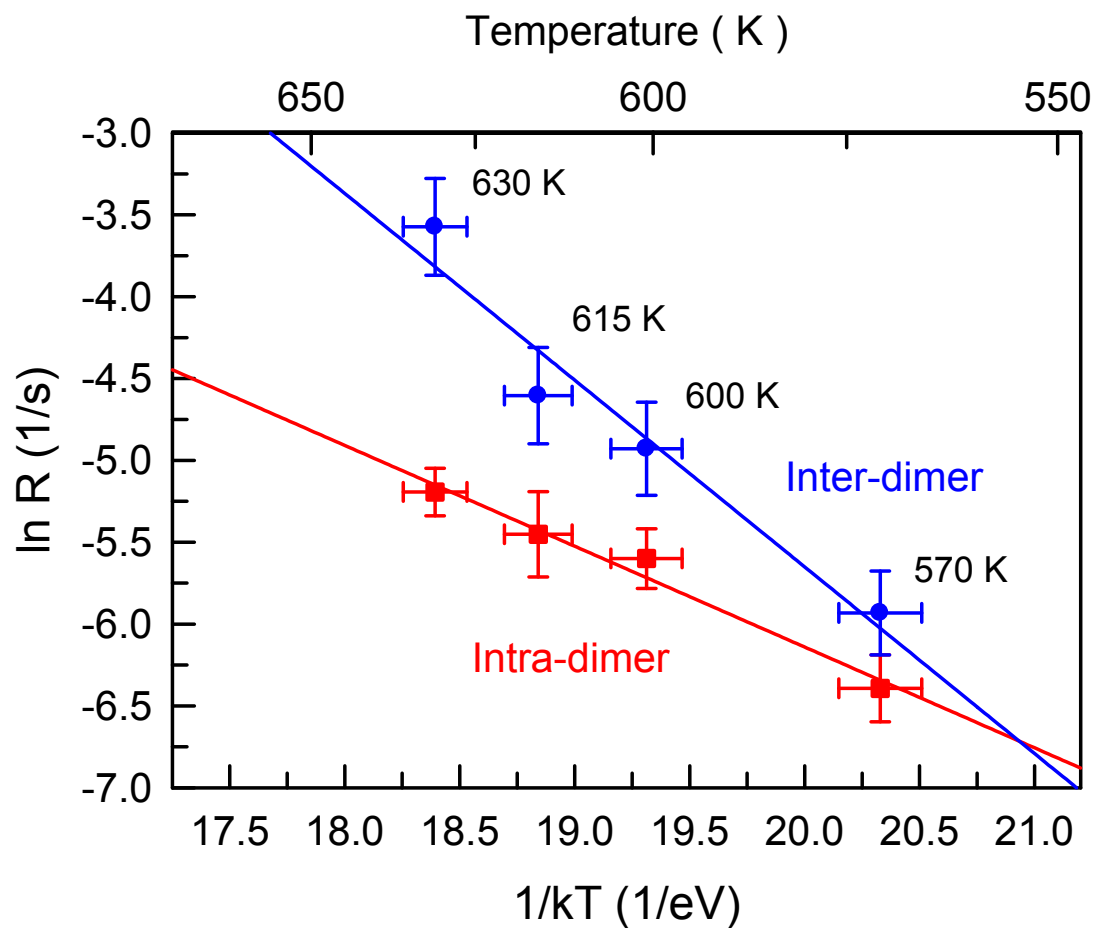


Fig.3.14 An Arrhenius plot of the non H-exposed hopping rates with lines from both inter-dimer and intra-dimer directions plotted separately. From the gradient of the plot we obtained the activation energies as  $1.14\text{eV}$  and  $0.62\text{eV}$ , and from the y-axis intercept we obtained the frequency prefactors as  $2.83 \times 10^7 \text{ s}^{-1}$  and  $4.83 \times 10^2 \text{ s}^{-1}$  for the inter-dimer and intra-dimer hoppings respectively.

### 3.4 Conclusion

From the three hopping dynamics we saw them as independent mechanisms and treated them separately. Because inter-dimer and intra-dimer hoppings were most often observed while inter-row hoppings were rare, therefore we only look at the two basic dynamics. By carefully tracing the single hydrogen sites in each temperature sets we found the average hopping rates for the dynamics from the various sets.

We have found similar results from both set of the samples as with and without the exposure of H. The statistics we have done showed an agreement in the behavior of the dark sites. The plots also showed a very similar trend of the lines for both cases. From the calculated values of both sets we are able to correspond it with our earlier results. The activation energies calculated from each set roughly agree with each other, with only a minor difference between the two. The frequency prefactors were also in an acceptable range. Therefore, it can now prove that our assumptions were correct and those “vacancies” saw moving on the non H-exposed Si(100) Cl-terminated (2x1) surface could have been the residual hydrogen atoms inside the vacuum chamber and got onto the surface during sample preparation and/or from the  $HCl$  impurities in the  $Cl_2$  gas source. The transporting mechanism of these single hydrogen atoms was simply the exchange of positions between the hydrogen sites and the adjacent chlorine sites.



## Chapter 4 Conclusions

In this thesis, we have done experiments on Si(100) Cl-terminated surfaces in order to prove our assumptions about the “single vacancies” being seen moving on the Si surfaces. For long we have thought these “vacancies” were just defects on the surface, but experimental results have shown otherwise. Decades since scientists first began doing researches on Si(100) surfaces, but only a few had looked at the dynamic events happening with the “vacancies” on the Si(100) Cl-terminated surfaces. In this, we have focused on the phenomena and obtained some interesting results which solved our query.

We started by exposing hydrogen atoms on the Si(100) Cl-terminated surface. By exposing more hydrogen gas onto the surface, more dark sites were created. We then heat the sample by adding currents to the sample until we have obtained the desired temperature. We took images of the H-exposed Cl-terminated surface at temperatures 570K, 600K, 615K, 639K and 650k for an average period of 30 minutes and traced the single hydrogen atoms in defined zones respectively. By defining the zone of trace we were able to observe the interactions between the hydrogen and chlorine atoms. Following is a brief summary of our findings:

1. We have identified the exchanging motions between the atoms as three types:
  - a. Intra-dimer,
  - b. Inter-dimer (Intra-row), and
  - c. Inter-row.
2. We have shown the behavior of single hydrogen atoms at temperatures 570K~650K.
3. From all experiments, very few inter-row hoppings were found, as expected. It only counted 0.5~1 percent in the overall hopping observations. It was believed that a much higher energy was needed for atoms to overcome the energy barrier and jump cross the dimer rows. Therefore only a few can have that amount of energy at lower temperatures while it was easier to obtain at higher temperatures.
4. From the statistical results conducted, in the case of inter-dimer hoppings, no preference was found as motions in both left and right directions were equally likely to happen. But the multiple step jumps were temperature dependent, as the temperature rises, multiple jumps were more likely to happen, and the distance of the jumps increases.
5. From the average hopping rates calculated for each set, it shows a steady climb in the rate as the temperature rises.

6. We have obtained the activation energy and the attempt frequency prefactor for the H-exposed data set as:

	Inter-dimer	Intra-dimer
$E_a$ (eV)	1.23	0.70
$P$ ( $s^{-1}$ )	$6.37 \times 10^7$	$1.28 \times 10^3$

While for the non H-exposed set was:

	Inter-dimer	Intra-dimer
$E_a$ (eV)	1.14	0.62
$P$ ( $s^{-1}$ )	$2.83 \times 10^7$	$4.83 \times 10^2$

7. From the results obtained we were able to conclude that, as the calculated values from each cases roughly in agreement, our initial assumptions can then be confirmed as valid and the “vacancies” we have been observing on the non H-exposed Si(100)-(2x1) Cl-terminated surface were actually residual hydrogen atoms got on the surface during sample preparation and/or from the  $HCl$  impurity in the  $Cl_2$  gas source.

In the future work, we expect to shorten our time for obtaining the images by increasing our scanning speed and also decrease the size of area to be scanned. This way we will have a better and more accurate data statistics for the calculation of prefactors and the activation energies. Investigations on the lower temperatures are also an aspect we need to look at which might help us in understanding more about the details of the atom movement.

# Appendix A

## A.1 Previous experimental results

In one of the experiment we have done earlier, we have obtained some of the results corresponds to the mentioned experiment we have done in chapter 3. The experiment was also done on the Si(100) Cl-terminated surface. After heating the sample at 500mA, which was about 520K, we observed the surface. We find that there was hopping events happening on the surface and so we recorded our data. We then heated the sample up to 550mA, which was about 565K, and again observed the surface for site hoppings. Both temperatures were determined by infrared thermometer (IR thermometer).

We traced about 30 single dark sites in a period of 1.5~2 hours and observed their movements. As usual, we plotted our calculated results for the energy barrier with Arrhenius relations; we obtained a result of 0.67eV for the activation energy and  $7.69 \times 10^3 s^{-1}$  for the prefactor (fig A.1). This result was calculated by mixing the two dynamics, as inter-dimer hoppings and intra-dimer hoppings were added together and treated the same. So with the uncertainty about the exact temperature, therefore this result might not be as accurate as we hoped and can only be as a reference. However, from the statistics point of view, we summed up the experiment data with a closer observation on the motions of the H-hoppings. Interested on how the sites preferred to move on the surface, we found surprisingly that under the inter-dimer dynamic, the preference of movements was almost equal in both directions (fig A.2). These have now been supported by our later calculated results which were shown agreeing to these results.

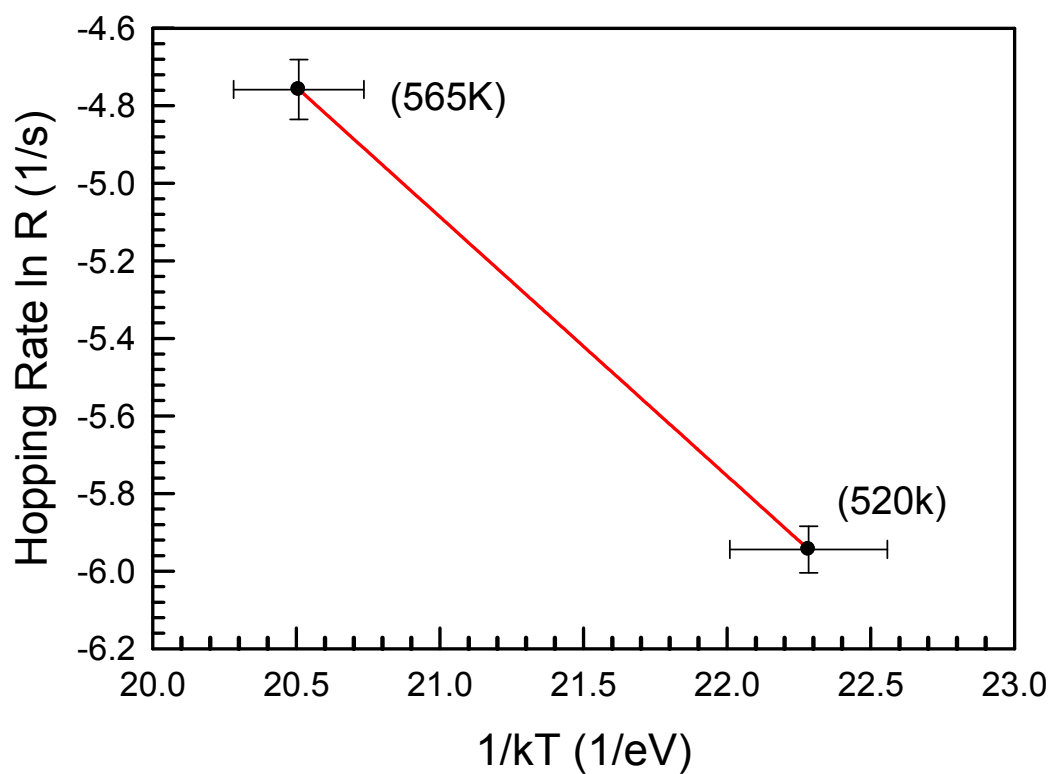


Fig. A.1 An Arrhenius plot with the hopping rates of single vacancy jumps. We obtained a result of 0.67eV for the activation energy and  $7.69 \times 10^3 s^{-1}$  for the prefactor.

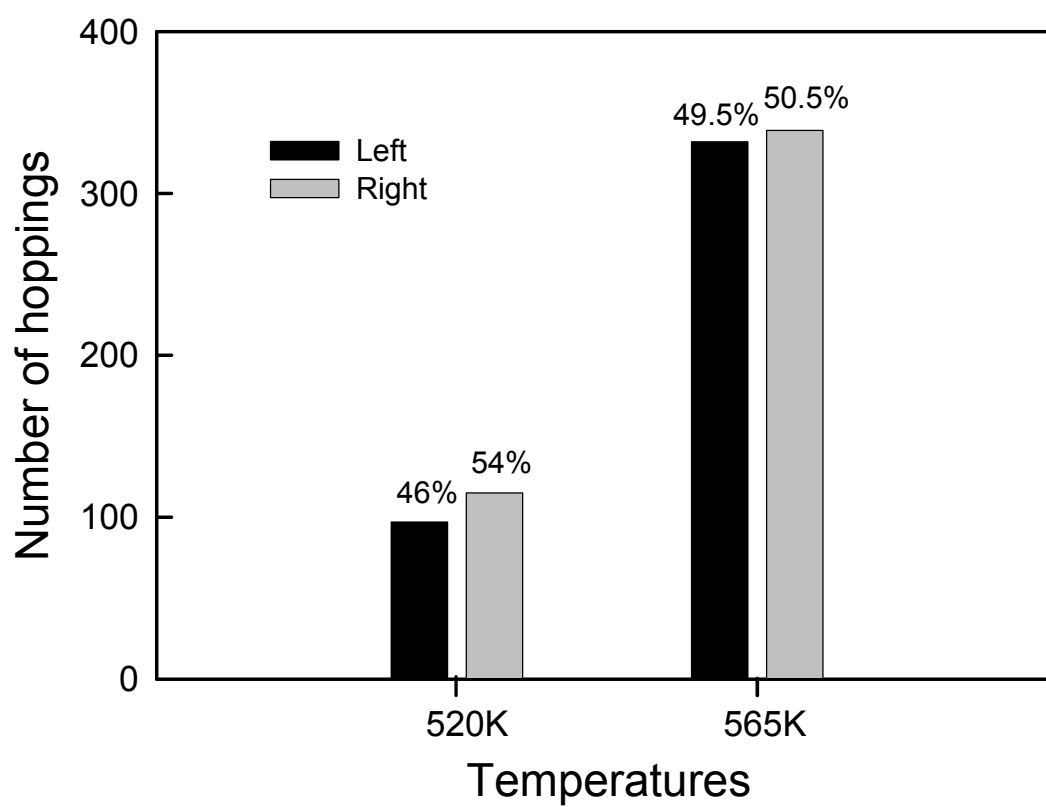
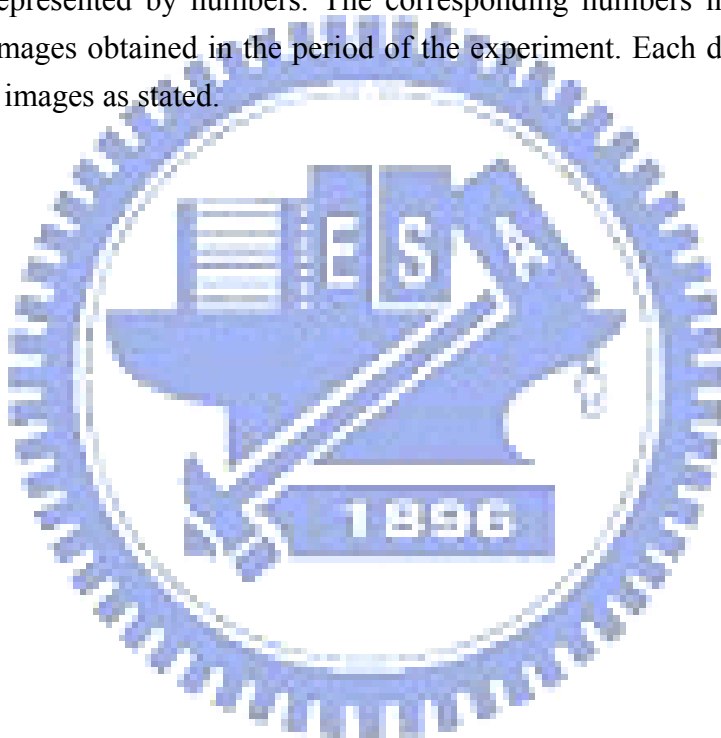


Fig. A.2 A chart showing the percentages at both temperatures the direction of movement which was preferred in the inter-dimer dynamic.

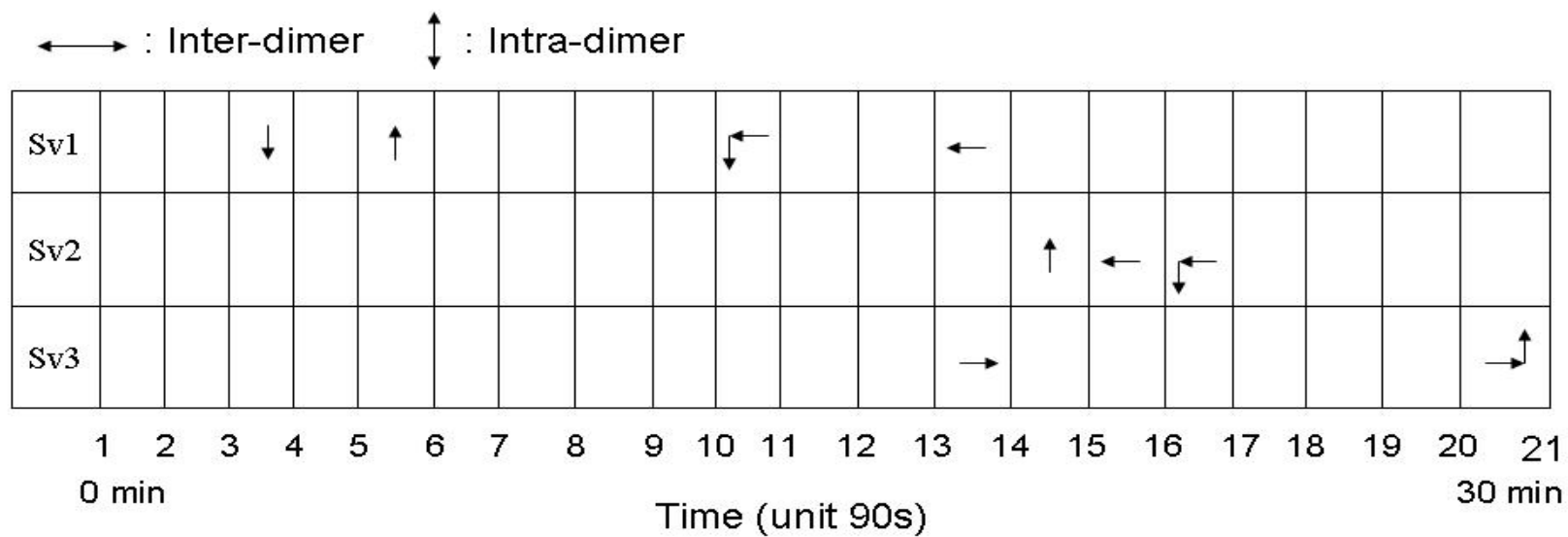
## Appendix B

### B.1 Flow charts

From each of the three temperature sets 570, 600 and 630K of the H-exposed data sets we picked three single atoms that was counted and drew up a flow chart showing their recorded movements. The atoms traced were plotted with up-down and left-right arrows representing the two motion dynamics, in which up-down means moving in the direction inside a dimer (intra-dimer), while left-right means moving in the left or right direction in a dimer row (inter-dimer). A single arrow symbolizes a single jump, while jumps larger than four were represented by numbers. The corresponding numbers in the x-axis means the number of images obtained in the period of the experiment. Each data set has a delta time between the images as stated.

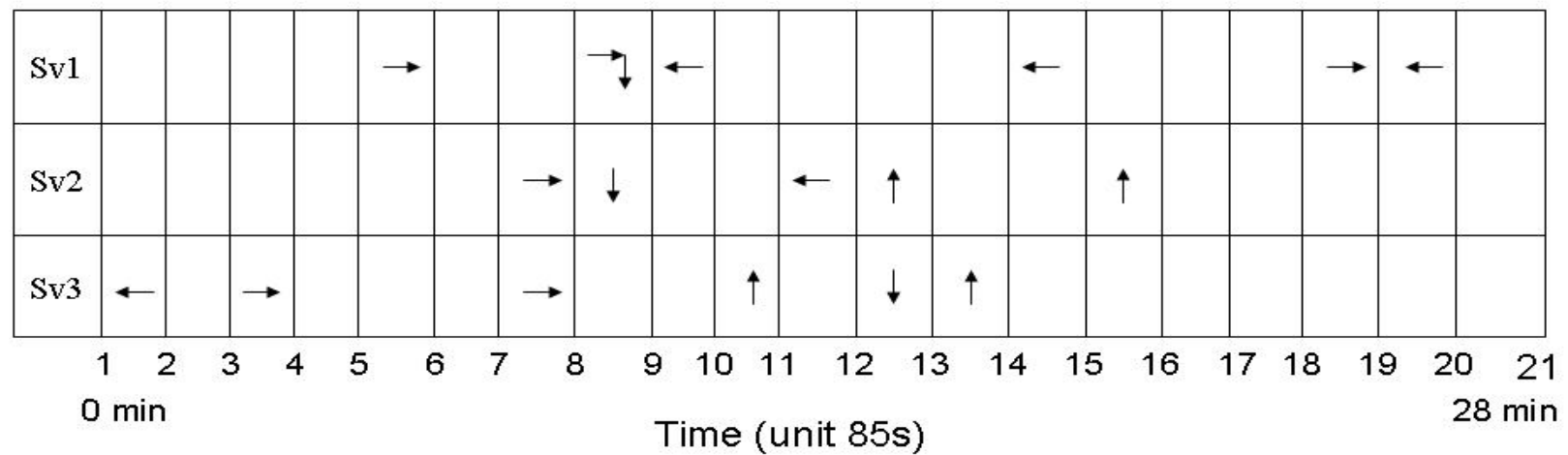


## Flow chart of Si(100) sample with H-exposure at 570K



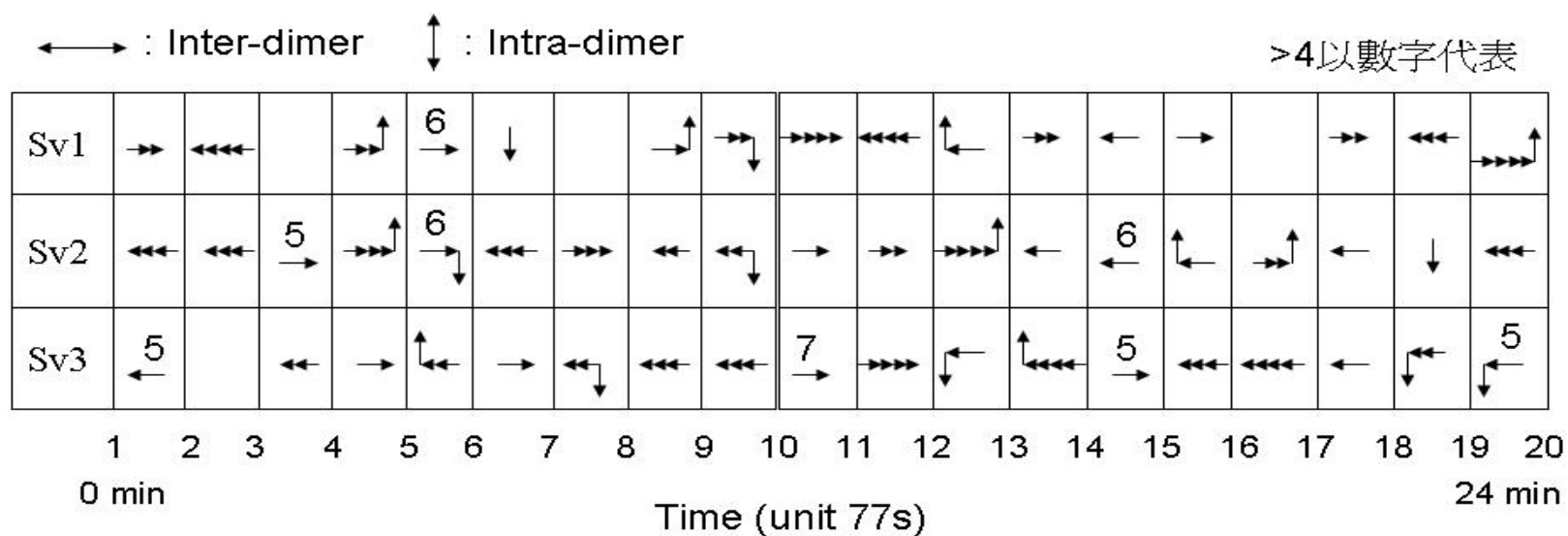
## Flow chart of Si(100) sample with H-exposure at 600K

$\longleftrightarrow$  : Inter-dimer       $\updownarrow$  : Intra-dimer





## Flow chart of Si(100) sample with H-exposure at 630K



## References

- [1] R.M. Tromp, R. J. Hamers, and J.E. Demuth, *Phys. Rev. Lett.* **55**, 1303 (1985).
- [2] N. Roberts and R. J. Needs, *Surf. Sci.* **236**, 112 (1990).
- [3] J. Wang, T. A. Arias, and J. D. Joannopoulos, *Phys. Rev. B* **47**, 10497 (1993).
- [4] G. Kellogg, *Surf. Sci.* **246**, 31 (1991).
- [5] S. Wang, J. Wrigley, and G. Ehrlich, *J. Chem. Phys.* **91**, 5087 (1989).
- [6] M. Lovisa and G. Ehrlich, *J. Phys.* **50**, C8-279 (1989).
- [7] R. Ferrando, R. Spadacini, G. E. Tommei, and G. Carrati, *Surf. Sci.* **311**, 411 (1994).
- [8] D. Senft and G. Ehrlich, *Phys. Rev. Lett.* **74**, 294 (1995).
- [9] T. Flores, S. Junghans, and M. Wuttig, *Surf. Sci.* **371**, 1 (1997).
- [10] I. Brihuega, O. Custance, and J. Gomez-Rodriguez, *Phys. Rev. B* **70**, 165410 (2004).
- [11] R. van Gastel, E. Somfai, W. van Saarloos, and J. Frenken, *Nature* **408**, 665 (2000).
- [12] R. van Gastel, E. Somfai, W. van Saarloos, and J. Frenken, *Surf. Sci.* **521**, 10 (2002).
- [13] D.-S. Lin, E. Hirschorn, T.-C. Chiang, R. Tsu, D. Lubben, and J. Green, *Phys. Rev. B* **45**, 3494 (1992).
- [14] R. Stumpf, *Phys. Rev. B* **53**, R4253 (1996).
- [15] G. Kellogg, *Phys. Rev. B* **55**, 7206 (1997).
- [16] J. Nara, T. Sasaki, and T. Ohno, *Phys. Rev. Lett.* **79**, 4421 (1997).
- [17] S. Horch, H. Lorensen, S. Helveg, E. Laegsgaard, I. Stensgaard, K. Jacobsen, J. Norskov, and F. Besenbacher, *Nature* **398**, 134 (1999).
- [18] M.-F. Hsieh, J. Y. Chung, D.-S. Lin, and S.-F. Tsay, to be published.
- [19] N. Kitamura, M. Lagally, and M. Webb, *Phys. Rev. Lett.* **71**, 2082 (1993).
- [20] J. Owen, D. Bowler, C. Goringe, K. Miki, and G. Briggs, *Phys. Rev. B* **54**, 14153 (1996).
- [21] G. Kellogg, *Surf. Sci. Rep.* **21**, 1 (1994).

- [22] R.Tromp, *Nature Mat.* **2**, 212 (2003).
- [23] J. Iguain, and H. Martin, *Phys. Rev. B* **54**, 8751 (1996).
- [24] B. Swartzentruber, *Phys. Rev. Lett.* **76**, 459 (1996).
- [25] T. Linderoth, S. Horch, E. Laegsgaard, I. Stensgaard, and F. Besenbacher, *Phys. Rev. Lett.* **78**, 4978 (1997).

